Ullah, S. N. *et al*. (2017). *Géotechnique* **67**, No. 8, 672–690 [http://dx.doi.org/10.1680/jgeot.16.P.101]

# Foundation punch-through in clay with sand: analytical modelling

S. N. ULLAH*, S. STANIER†, Y. HU‡ and D. WHITE†

Severe punch-through of jack-up rig foundations can occur due to the presence of a stronger sand layer in a bed of relatively soft clay. Analytical estimation of the bearing capacity and leg load–penetration response on such multi-layer stratigraphies is challenging. Accurate mechanism-based models need to be established in each of the layers involved and the effects of the mechanisms in each of the layers on the response in the other layers must be captured. Based on the recently developed failure stress-dependent punch-through models for sand–clay stratigraphies, an extended model is proposed for clay–sand–clay stratigraphies. Half-spudcan particle image velocimetry centrifuge tests and full-spudcan centrifuge tests are used in developing and validating the extended model. The centrifuge test results were discussed in a companion paper and this paper focuses on the analytical developments and prediction assessment. Both spudcan peak resistance ($q_{peak}$) and spudcan punch-through depth ($d_{punch}$) can be estimated using the model. The predictions by the extended model and by the current industry guidelines are compared against the centrifuge test data. The extended model proposed in this paper outperforms the approaches suggested in the guidelines. An advantage of the proposed approach is that it can be used for either sand–clay or clay–sand–clay scenarios and exhibits excellent performance compared to the model testing dataset considered in this work for both cases. The resulting penetration resistance model is a useful design tool for routine punch-through risk assessment.

KEYWORDS: bearing capacity; centrifuge modelling; footings/foundations; model tests; offshore engineering; soil/structure interaction

## INTRODUCTION

Oil and gas recovery in shallow to medium water depths (up to ~150 m) is commonly carried out from self-elevating jack-up rigs. Jack-up rigs are supported by quasi-circular or sometimes polygonal shaped foundations, commonly referred to as spudcans. Punch-through of spudcan foundations remains the most common cause of failure of jack-up rig deployment (Osborne & Paisley, 2002). Installation of spudcan foundations in clay with interbedded sand (clay–sand–clay profile) can lead to catastrophic punch-through failure, where the foundation leg penetrates uncontrollably for several metres before stabilising in the underlying clay (Fig. 1). Such stratigraphies are common to many offshore sites such as the Gulf of Suez, Southeast Asia, Gulf of Mexico and offshore South America (Baglioni *et al*., 1982; Dutt & Ingram, 1984; Teh *et al*., 2009) and have led to fatalities among operational personnel (Dier *et al*., 2004).

Accurate models for predicting the peak resistance during punch-through failure on sand–clay stratigraphies have been developed (Fig. 2). Lee *et al*. (2013a) conducted centrifuge experiments and small-strain finite-element (FE) numerical simulations for dense sand (relative density, $I_D = 92\%$) overlying clay resulting in the development of a simplified conceptual model to predict the peak punch-through capacity, $q_{peak}$ (see Lee *et al*. (2013b) and Fig. 2(a)). Hu *et al*. (2014a) modified the model further to account for the depth of embedment during mobilisation of the peak resistance (Fig. 2(b)) and validated the model for medium dense sand on clay ($I_D = 44\%$). Simple methods for predicting the penetration resistance profile for sand–clay stratigraphies have also been proposed (Hu *et al*., 2014b).

However, no validated analytical model exists for stratigraphies involving more than two layers. The current industry guidelines (Sname, 2008; ISO, 2012) recommend soil models originally developed for two layers (either the punch-through model for strong over soft soil such as sand–clay, or the squeezing model for soft over strong soil such as clay–sand). However, no specific guidelines are provided for the application of these methods for either clay–sand–clay or sand–clay–sand scenarios. Furthermore, these basic models have already been shown to generate poor predictions for sand–clay stratigraphies (Hu *et al*., 2015a), primarily because of their inability to account for the stress-level-dependent behaviour of sand (i.e. the friction angle changing with ambient stress level). In addition, image analysis of multi-layered punch-through centrifuge experiments (see Teh *et al*., 2008; Hossain, 2014; Hu *et al*., 2015b; Ullah *et al*., 2017) indicate that some of the overlying soil becomes entrapped beneath the spudcan foundation during penetration, leading in some instances to increased penetration resistance but a less severe punch-through event. The simple models recommended by the Society for Naval Architects and Marine Engineers (Sname) and the International Organization for Standardization (ISO) do not account for these entrapped layers of soil, causing the models to significantly underpredict the penetration resistance during punch-through, and often to overpredict the risk associated with uncontrolled leg penetration (Ullah *et al*., 2017).

This paper develops an analytical method to predict the penetration resistance profile for jack-up foundations on clay–sand–clay stratigraphies, which can be generalised to higher numbers of layers. The method incorporates simple

Manuscript received 13 April 2016; revised manuscript accepted 25 November 2016. Published online ahead of print 16 January 2017. Discussion on this paper closes on 1 January 2018, for further details see p. ii.

* Department of Civil and Environmental Engineering, National University of Singapore, Singapore; formerly Centre for Offshore Foundation Systems, University of Western Australia, Crawley, WA, Australia.
† Centre for Offshore Foundation Systems, University of Western Australia, Crawley, WA, Australia.
‡ School of Civil Environmental and Mining Engineering, University of Western Australia, Crawley, WA, Australia.

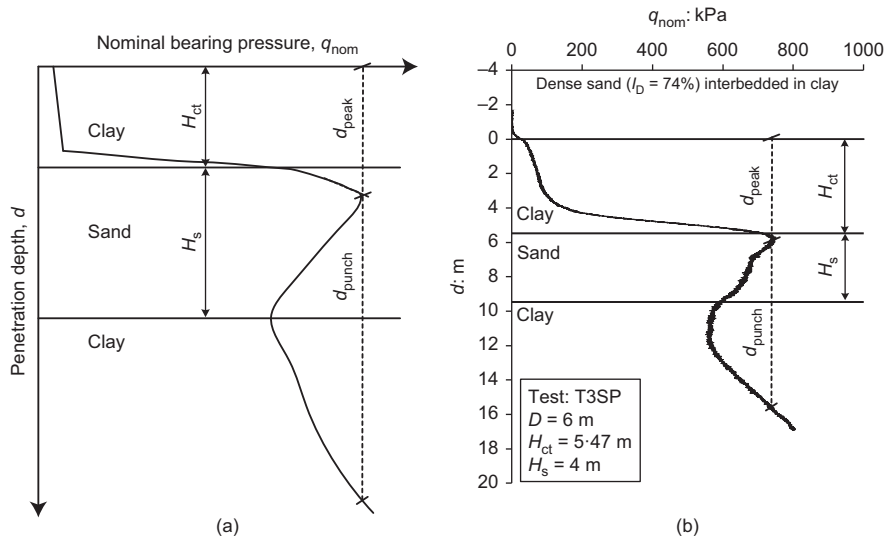


**Fig. 1. (a) Typical load–penetration response in clay–sand–clay stratigraphy and (b) centrifuge test data in clay–sand–clay after Ullah *et al.* (2017)**

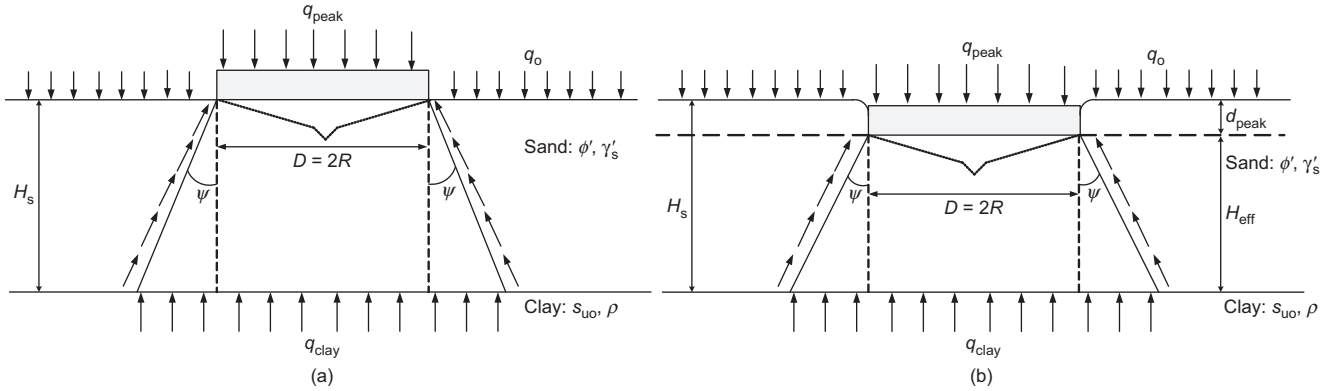


**Fig. 2. Recent analytical models of punch-through on sand overlying clay: (a) mechanism of Lee *et al.* (2013b); (b) mechanism of Hu *et al.* (2014a)**

models for the penetration resistance in the top clay layer, the peak resistance in the sand layer and the penetration resistance in the underlying clay layer. The models in different layers are developed based on the failure mechanisms observed in the experiments in which image analysis was used to determine the soil deformation patterns (White *et al.*, 2003; Stanier *et al.*, 2016) (see Fig. 3). The peak resistance model incorporates a modified version of Bolton's equations (Bolton, 1986) to capture the stress-level-dependent response of the sand layer during punch-through. Moreover, the peak resistance model extends the approaches reported by Lee *et al.* (2013b) and Hu *et al.* (2014a), where the top clay layer height is zero. In this way, the clay–sand–clay model developed here can be easily simplified to the two-layer model without the top clay layer (i.e. sand–clay), assuming that for both the soil stratigraphies the sand and clay shearing is in a drained and undrained manner, respectively. All models are formulated in terms of soil parameters that have clear physical meanings and can be determined from standard offshore investigations. The method is validated against a series of centrifuge model tests that covers a range of clay–sand–clay layer geometries and soil properties.

## EXTENDED STRESS-DEPENDENT MODEL FOR $q_{peak}$

The primary calculation when assessing punch-through potential for stratigraphies involving thin sand layers is the peak resistance mobilised in the sand layer ($q_{peak}$), as loading the jack-up foundation to a level higher than this pressure usually initiates the punch-through failure if the underlying layers are comparably weak. When assessing the potential severity of punch-through failure, the bearing capacity in the over- and underlying clay layers must also be predicted to form a complete penetration response, which will be discussed later in this paper. Based on the complete penetration profile of the spudcan, the punch-through depth can be determined, when an equilibrium is re-established in the underlying weaker layer and punch-through failure ceases.

The $q_{peak}$ model for clay–sand–clay is an extension to the sand–clay model of Hu *et al.* (2014a). The geometry of the mechanism is based on observations of soil deformation described in the companion paper (Ullah *et al.*, 2017) and is illustrated in Fig. 4. In essence, a frustum of sand underneath the spudcan punches through into the underlying clay layer with the spudcan. The sand frustum has a spreading angle to the vertical approximately equal to the dilation angle ($\psi$) of the sand. The mechanism of three layers (clay–sand–clay) is similar to that of two layers (sand–clay) described by Hu *et al.* (2014a) with the following additions.

(*a*) A layer of clay of height $H_c$ is entrapped between the spudcan and the sand frustum, based on the soil deformation observations of Ullah *et al.* (2017).

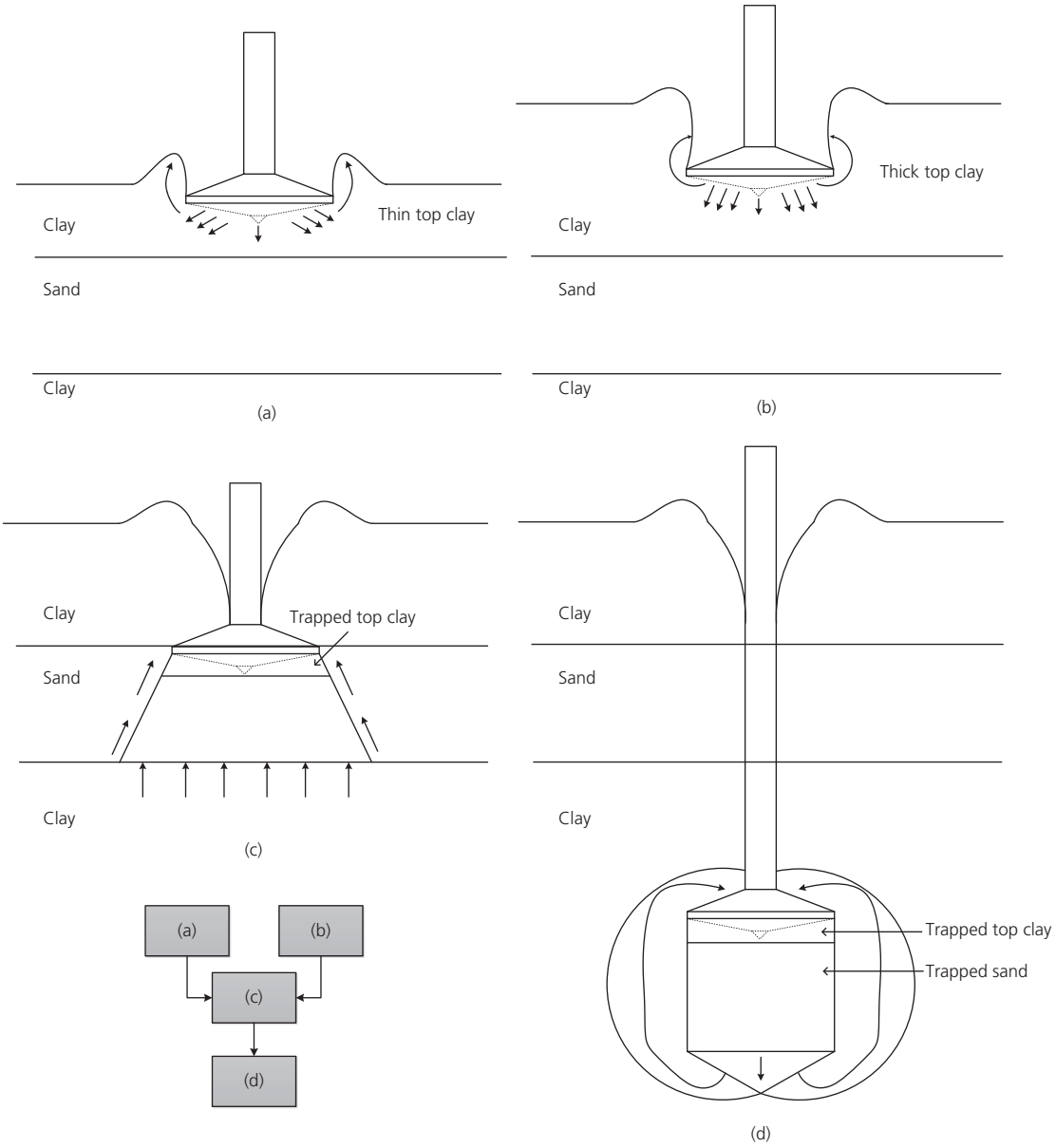


**Fig. 3. Summary of soil flow mechanisms in clay–sand–clay: (a) squeezing of thin clay layer; (b) bearing failure of thick clay layer; (c) peak resistance in sand layer; (d) bearing capacity of the composite spudcan, clay and sand plug in the underlying clay layer**

(*b*) As a result, the depth at which the peak resistance is mobilised, $d_{\text{peak}}$, is less than that for the two-layer sand–clay case.
(*c*) Partial backflow of the top layer of clay above the spudcan occurs prior to the mobilisation of $q_{\text{peak}}$.

The following sections describe how these additions are considered in the three-layer (clay–sand–clay) model based on the two-layer (sand–clay) model of Hu *et al.* (2014a).

## MATHEMATICAL FORMULATION FOR PEAK RESISTANCE $q_{\text{peak}}$

Based on vertical equilibrium of a thin horizontal disc element (Fig. 4(b)) the following differential equation is formed (following Lee *et al.* (2013b) and Hu *et al.* (2014a))

$$\frac{\mathrm{d}\sigma'_z}{\mathrm{d}z} + \frac{2[\tan\psi + D_{\text{F}}(\tan\phi^* - \tan\psi)]\sigma'_z}{R + z\tan\psi} - \gamma'_{\text{s}} = 0 \qquad (1)$$

$D_{\text{F}}$ is the ratio between the effective normal stresses acting on the sides of the sand frustum and the mean vertical stress within the frustum. Mathematically

$$D_{\text{F}} = \frac{\sigma'_{\text{n}}}{\sigma'_z} \qquad (2)$$

$\phi^*$ is a reduced friction angle due to non-associated flow of sand, obtained from the expression proposed by Drescher & Detournay (1993) as

$$\tan\phi^* = \frac{\sin\phi'\cos\psi}{1 - \sin\phi'\sin\psi} \qquad (3)$$

Following Lee *et al.* (2013b) and Hu *et al.* (2014a), equation (1) can be simplified by introducing a simplification parameter $E$

$$\frac{\mathrm{d}\sigma'_z}{\mathrm{d}z} + \frac{E\tan\psi\sigma'_z}{R + z\tan\psi} - \gamma'_{\text{s}} = 0 \qquad (4)$$

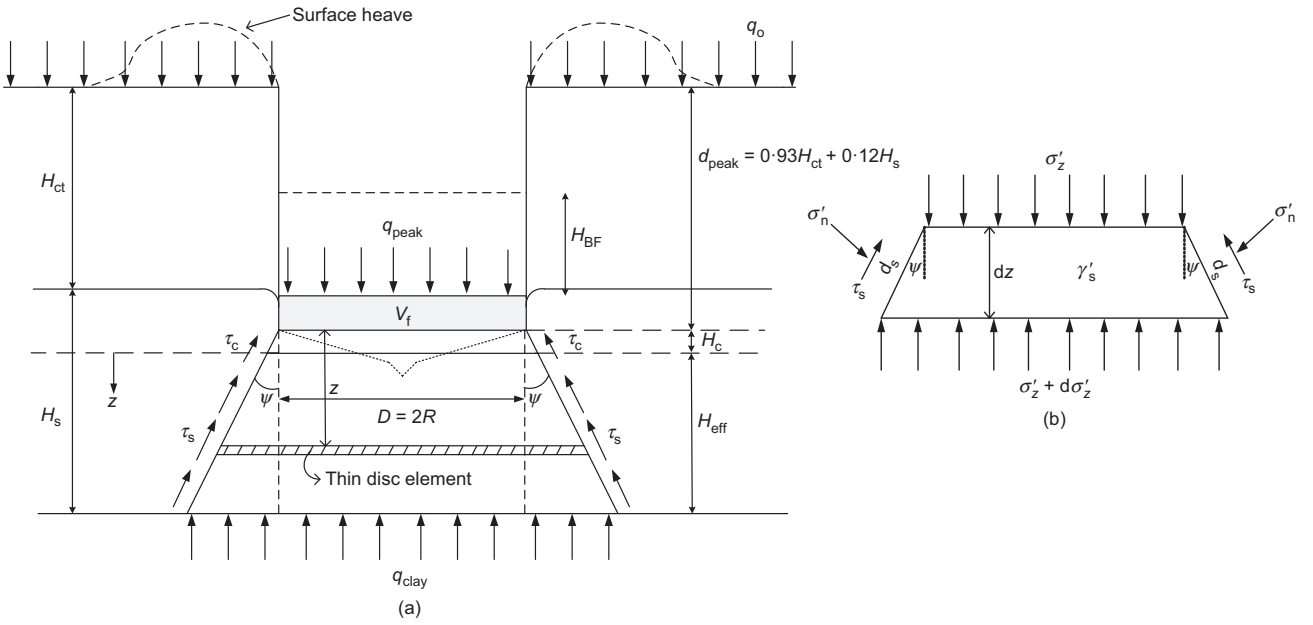


**Fig. 4. Peak resistance model: (a) idealised failure mechanism for clay–sand–clay stratigraphies; (b) forces acting on an infinitesimally thin disc element**

where

$$E = 2\left[1 + D_F\left(\frac{\tan\phi^*}{\tan\psi} - 1\right)\right] \tag{5}$$

The stress ratio of $D_F$ was related to the normalised height of the sand layer ($H_s/D$) based on the empirical study by Hu *et al*. (2015c). This empirical power law is also adopted here

$$D_F(\text{spudcan}) = 0{\cdot}642\left(\frac{H_s}{D}\right)^{-0{\cdot}576}; \quad 0{\cdot}16 \le \frac{H_s}{D} \le 1{\cdot}0 \tag{6}$$

$$D_F(\text{flat}) = 0{\cdot}623\left(\frac{H_s}{D}\right)^{-0{\cdot}174}; \quad 0{\cdot}21 < \frac{H_s}{D} < 1{\cdot}12 \tag{7}$$

Equations (6) and (7) provide a slightly higher value of $D_F$ for a spudcan. The higher $D_F$ value for a spudcan reflects the probable generation of increased lateral stresses during $q_{peak}$ mobilisation due to the conical underside, as illustrated in Lee *et al*. (2013b), which was also demonstrated by the higher accumulated radial strains underneath the spudcan by Hu *et al*. (2015b).

Equation (1) can be directly integrated by assuming $E$ is constant to give the following form

$$(R + z\tan\psi)^E \sigma'_z = \frac{\gamma'_s(R + z\tan\psi)^{E+1}}{\tan\psi(E+1)} + C \tag{8}$$

where $C$ is the integration constant and can be evaluated from the first boundary condition as: at $z = H_{eff}$, the vertical stress $\sigma'_z$ equates to the bearing capacity of the underlying clay layer $q_{clay}$ (Fig. 4). The bearing capacity of the underlying clay $q_{clay}$ is defined after Lee *et al*. (2013b) as

$$q_{clay} = N_{co}s_{ubi} + q_o + H_{ct}\gamma'_{ct} + H_{eff}\gamma'_s + 0{\cdot}12H_s\gamma'_s + \text{sign}(H_{ct})\frac{4V_f}{\pi D^2}\gamma'_{ct} \tag{9}$$

where $s_{ubi}$ is the bottom intercept strength; $q_o$ is the surcharge; and $\gamma'_{ct}$ and $\gamma'_s$ are the top clay and sand effective unit weights, respectively. The last term of equation (9) is attributable to surface heave where $V_f$ is the volume of the embedded foundation. Soil deformation observations of Teh *et al*. (2008) showed that the sand around the periphery of the spudcan did not heave, so the last term is taken as zero when $H_{ct}$ is zero (i.e. sign(0) = 0). When $H_{ct} = 0$ equation (9) reduces to the clay bearing capacity for sand–clay stratigraphies, and when $H_s$ is zero (i.e. $H_{eff}$ is also zero) the bearing capacity of a single layer of clay is recovered.

The bearing capacity factor $N_{co}$ is obtained from expressions provided by Houlsby & Martin (2003) for a rough circular foundation as

$$N_{co} = 6{\cdot}34 + 0{\cdot}56\kappa \tag{10}$$

where $\kappa$ is the normalised bottom clay strength gradient and is taken as

$$\kappa = \frac{\rho_{cb}[D + 2(H_{eff} + H_c)\tan\psi]}{s_{ubi}} \tag{11}$$

where $\rho_{cb}$ is the bottom clay strength gradient and $\psi$ is the inclination from vertical of the failure surface in the sand layer (see Fig. 4), which is taken as equal to the sand dilatancy angle. $\kappa$ lies within $0 \le \kappa \le 5$. Equation (10) is the best fit of the tabulated data provided by Houlsby & Martin (2003) with a discrepancy always less than 5%.

Therefore, the integration constant $C$ can be evaluated as

$$C = (R + H_{eff}\tan\psi)^E\left[\left(N_{co}s_{ubi} + q_o + H_{ct}\gamma'_{ct} + H_{eff}\gamma'_s + 0{\cdot}12H_s\gamma'_s + \text{sign}(H_{ct})\frac{4V_f}{\pi D^2}\gamma'_{ct}\right) - \frac{\gamma'_s(R + H_{eff}\tan\psi)}{\tan\psi(E+1)}\right] \tag{12}$$

By substituting $C$ into equation (8), taking $H_{\text{eff}}$ as $0{\cdot}88H_{\text{s}}$ (after Ullah *et al.*, 2017), replacing foundation radius $R$ by $D/2$ and applying the second boundary condition as: at $z = -H_{\text{c}}$, the mean vertical stress ($\sigma'_z$) equates to the peak bearing capacity $q_{\text{peak}}$, then the peak resistance $q_{\text{peak}}$, where $\phi' > \phi_{\text{cv}}$, can be expressed as

$$\begin{aligned} q_{\text{peak}} = &\left[N_{\text{co}}s_{\text{ubi}} + q_{\text{o}} + 0{\cdot}12H_{\text{s}}\gamma'_{\text{s}} + H_{\text{ct}}\gamma'_{\text{ct}} + \text{sign}(H_{\text{ct}})\frac{4V_{\text{f}}}{\pi D^2}\gamma'_{\text{ct}}\right] \\ &\times \left(1 + \frac{1{\cdot}76H_{\text{s}}}{D}\tan\psi\right)^{E} + \frac{\gamma'_{\text{s}}D}{2\tan\psi(E+1)} \\ &\times \left[1 - \left(1 - \frac{1{\cdot}76H_{\text{s}}}{D}E\tan\psi\right)\left(1 + \frac{1{\cdot}76H_{\text{s}}}{D}\tan\psi\right)^{E}\right] \\ &+ (\tau_{\text{c}}\cos\psi - f_1 H_{\text{ct}}\gamma'_{\text{ct}} - f_2 H_{\text{ct}}\gamma'_{\text{ct}}) \le q_{\text{sand}}; \quad \text{for } \phi' > \phi_{\text{cv}} \end{aligned} \tag{13}$$

where $E$ is as defined in equation (5); $\tau_{\text{c}}$ is the shear stress generated by shearing along the periphery of the entrapped clay layer; and $f_1$ and $f_2$ are fractions of the top clay layer height. The factors $f_1$ and $f_2$ represent the fractions of the top clay layer height that become entrapped beneath the foundation and backflow onto the top of the foundation at mobilisation of the peak resistance, respectively.

The inequality at the end of equation (13) is to limit the bearing capacity to that of a circular foundation resting on a deep layer of sand ($q_{\text{sand}}$) with surcharge $q_{\text{o(s)}}$

$$q_{\text{sand}} = s_\gamma N_\gamma \frac{\gamma'_{\text{s}}D}{2} + s_q N_q q_{\text{o(s)}} \tag{14}$$

$$q_{\text{o(s)}} = q_{\text{o}} + H_{\text{ct}}\gamma'_{\text{ct}} + \text{sign}(H_{\text{ct}})\frac{4V_{\text{f}}}{\pi D^2}\gamma'_{\text{ct}} \tag{15}$$

where $s_\gamma$, $s_q$ and $N_\gamma$, $N_q$ in $q_{\text{sand}}$ are the shape and bearing capacity factors, respectively, which are taken from Hansen (1970).

The soil deformation analyses of Ullah *et al.* (2017) indicated that the average entrapped clay layer height $H_{\text{c}}$ was 7% of the top clay layer height; hence $f_1$ is recommended as 0·07. Similarly, on average, half of the top clay layer height flowed back onto the top of the foundations; hence $f_2$ is recommended as 0·5.

The shear stresses on the periphery of the entrapped clay beneath the foundation ($\tau_{\text{c}}$) are limited by the shear strength of the clay within the plug. The visualisation experiments indicated the entrapped clay consisted of a mix of soft material from near the mud line and stronger material from the sand surface (i.e. the upper clay–sand interface). For simplicity, the strength of the clay within the entrapped clay plug has been taken as the average strength of the top clay layer, thus

$$\tau_{\text{c}}\cos\psi = \frac{0{\cdot}28H_{\text{ct}}[s_{\text{um}} + (\rho_{\text{ct}}H_{\text{ct}})/2](D + 0{\cdot}07H_{\text{ct}}\tan\psi)}{D^2} \tag{16}$$

Substituting $\tau_{\text{c}}$ of equation (16), $f_1 = 0{\cdot}07$ and $f_2 = 0{\cdot}5$ into equation (13) yields

$$\begin{aligned} q_{\text{peak}} = &\left[N_{\text{co}}s_{\text{ubi}} + q_{\text{o}} + 0{\cdot}12H_{\text{s}}\gamma'_{\text{s}} + H_{\text{ct}}\gamma'_{\text{ct}} + \text{sign}(H_{\text{ct}})\frac{4V_{\text{f}}}{\pi D^2}\gamma'_{\text{ct}}\right] \\ &\times \left(1 + \frac{1{\cdot}76H_{\text{s}}}{D}\tan\psi\right)^{E} + \frac{\gamma'_{\text{s}}D}{2\tan\psi(E+1)} \\ &\times \left[1 - \left(1 - \frac{1{\cdot}76H_{\text{s}}}{D}E\tan\psi\right)\left(1 + \frac{1{\cdot}76H_{\text{s}}}{D}\tan\psi\right)^{E}\right] \\ &+ \left[\frac{0{\cdot}28H_{\text{ct}}(s_{\text{um}} + \rho_{\text{ct}}H_{\text{ct}}/2)(D + 0{\cdot}07H_{\text{ct}}\tan\psi)}{D^2} \right. \\ &\left. - 0{\cdot}07H_{\text{ct}}\gamma'_{\text{ct}} - 0{\cdot}5H_{\text{ct}}\gamma'_{\text{ct}}\right] \le q_{\text{sand}}; \quad \text{for } \phi' > \phi_{\text{cv}} \end{aligned} \tag{17}$$

The effective height of the sand layer (i.e. the height of the sand layer when mobilising $q_{\text{peak}}$, measured as an average across the diameter of the foundation) was on average 88% of the original height of the sand layer in this study. This measurement is in agreement with the previous investigations from two-layer sand–clay tests by Teh *et al.* (2008) and Hu *et al.* (2015a). Referring to the diagram in Fig. 4, the spudcan penetration depth at $q_{\text{peak}}$ is

$$d_{\text{peak}} = 0{\cdot}93H_{\text{ct}} + 0{\cdot}12H_{\text{s}} \tag{18}$$

This relationship implies that greater entrapped clay height ($H_{\text{c}}$) leads to reduced $d_{\text{peak}}$ because the entrapped clay effectively increases the foundation thickness causing earlier peak resistance mobilisation. If the top clay height $H_{\text{ct}}$ is set to zero, $H_{\text{c}}$ becomes zero and $d_{\text{peak}}$ simplifies to that suggested by Teh *et al.* (2010) for sand–clay stratigraphies.

*Peak resistance when $\phi' = \phi_{\text{cv}}$ (i.e. loose sand)*

For the case where $\phi' = \phi_{\text{cv}}$, then $\psi = 0$ and $q_{\text{peak}}$ can be calculated as

$$\begin{aligned} q_{\text{peak}} = &\left[N_{\text{co}}s_{\text{ubi}} + q_{\text{o}} + 0{\cdot}12H_{\text{s}}\gamma'_{\text{s}} + H_{\text{ct}}\gamma'_{\text{ct}} + \text{sign}(H_{\text{ct}})\frac{4V_{\text{f}}}{\pi D^2}\gamma'_{\text{ct}}\right]\text{e}^{E_{\text{o}}} \\ &+ 0{\cdot}88H_{\text{s}}\gamma'_{\text{s}}\left[\text{e}^{E_{\text{o}}}\left(1 - \frac{1}{E_{\text{o}}}\right) + \frac{1}{E_{\text{o}}}\right] \\ &+ \left[\frac{0{\cdot}28H_{\text{ct}}(s_{\text{um}} + \rho_{\text{ct}}H_{\text{ct}}/2)}{D} - 0{\cdot}07H_{\text{ct}}\gamma'_{\text{ct}} - 0{\cdot}5H_{\text{ct}}\gamma'_{\text{ct}}\right] \\ &\le q_{\text{sand}}; \quad \text{for } \phi' = \phi_{\text{cv}} \end{aligned} \tag{19}$$

where $E_{\text{o}}$ is taken as

$$E_{\text{o}} = 3{\cdot}52D_{\text{F}}\sin\phi_{\text{cv}}\frac{H_{\text{s}}}{D} \tag{20}$$

Equations (17) and (19) are mathematically equivalent when the dilation angle $\psi$ is close to zero.

*Peak resistance when $H_{\text{ct}} = 0$*

Substituting $H_{\text{ct}} = 0$ into equation (17), the equation for $q_{\text{peak}}$ when $\phi' > \phi_{\text{cv}}$ for two-layer sand overlying clay reduces to

$$\begin{aligned} q_{\text{peak}} = &(N_{\text{co}}s_{\text{ubi}} + q_{\text{o}} + 0{\cdot}12H_{\text{s}}\gamma'_{\text{s}})\left(1 + \frac{1{\cdot}76H_{\text{s}}}{D}\tan\psi\right)^{E} \\ &+ \frac{\gamma'_{\text{s}}D}{2\tan\psi(E+1)}\left[1 - \left(1 - \frac{1{\cdot}76H_{\text{s}}}{D}E\tan\psi\right)\right. \\ &\left.\times\left(1 + \frac{1{\cdot}76H_{\text{s}}}{D}\tan\psi\right)^{E}\right] \le q_{\text{sand}} \end{aligned} \tag{21}$$

Equation (21) is identical to that proposed by Hu *et al.* (2014a), demonstrating that the three-layer model extension developed in this paper is universally applicable to both sand–clay and clay–sand–clay stratigraphies.

Similarly, setting $H_{\text{ct}} = 0$ in equation (19), the equation for $q_{\text{peak}}$ where $\phi' = \phi_{\text{cv}}$ reduces to

$$\begin{aligned} q_{\text{peak}} = &(N_{\text{co}}s_{\text{ubi}} + q_{\text{o}} + 0{\cdot}12H_{\text{s}}\gamma'_{\text{s}})\text{e}^{E_{\text{o}}} \\ &+ 0{\cdot}88H_{\text{s}}\gamma'_{\text{s}}\left[\text{e}^{E_{\text{o}}}\left(1 - \frac{1}{E_{\text{o}}}\right) + \frac{1}{E_{\text{o}}}\right] \le q_{\text{sand}} \end{aligned} \tag{22}$$

where $E_{\text{o}}$ is given by equation (20). This form is also identical to that given by Hu *et al.* (2014a) for loose sand–clay stratigraphies where $\phi' = \phi_{\text{cv}}$.

**Table 1. Parameters required for predicting peak resistance, $q_{peak}$**

| Parameter category | Symbol | Description | Method of determining parameter |
|---|---|---|---|
| Foundation geometry | $D$ and $V_f$ | Foundation diameter and volume | Known parameters |
| Top clay | $H_{ct}$ | Top clay height | Measured in situ |
| | $H_c$ | Height of trapped clay | Taken as $f_1 H_{ct}$ with $f_1 = 0{\cdot}07$ |
| | $s_{um}$ | Mud line undrained shear strength | Measured in situ or in laboratory tests |
| | $\rho_{ct}$ | Top clay strength gradient | Measured in situ |
| | $\gamma'_{ct}$ | Top clay unit weight | Inferred from in situ tests or directly measured in the laboratory |
| | $f_1$ | Factor determining the amount of top clay entrapment | Taken as 0·07, suggesting on average 7% of the top clay gets entrapped under the foundation |
| | $f_2$ | Factor determining the height of backfill | $f_2$ is taken as 0·50 (half backfill condition) |
| Sand | $H_s$ | Sand height | Measured in situ |
| | $I_D$ | Sand relative density | Measured in the laboratory from undisturbed samples or in situ |
| | $Q$ | Parameter in Bolton (1986) equation | Measured from laboratory tests, for siliceous sand can be taken as 10 |
| | $I_R$ | Relative density index | Obtained through an iterative procedure involving equations (17), (23), (24) and (25) |
| | $\varphi_{cv}$ | Constant volume friction angle | Measured from laboratory tests |
| | $\phi'$ and $\psi$ | Operative friction and dilation angle | Obtained from equations (24) and (25): $\phi' = \phi_{cv} + 2{\cdot}65 I_R$ and $0{\cdot}8\psi = \phi' - \phi_{cv}$, $\psi \geq 0$ |
| | $\phi^*$ | Reduced friction angle due to non-associated flow of sand | Obtained from equation (3): $\tan\phi^* = \dfrac{\sin\phi' \cos\psi}{1 - \sin\phi' \sin\psi}$ |
| | $\gamma'_s$ | Effective unit weight of sand | Inferred from in situ tests or directly measured in the laboratory |
| Bottom clay | $s_{ubi}$ | Bottom sand–clay intercept strength | Measured in situ |
| | $\rho_{cb}$ | Bottom clay strength gradient | Measured in situ |
| | $\kappa$ | Non-dimensional strength parameter needed to determine the bearing capacity factor from (Houlsby & Martin, 2003) | Calculated from equation (11): $\kappa = \dfrac{\rho_{cb}[D + 2(H_{eff} + H_c)\tan\psi]}{s_{ubi}}$; $H_{eff}$ is taken as $0{\cdot}88 H_s$ |
| | $N_{co}$ | Bottom clay bearing capacity factor | Calculated from equation (10): $N_{co} = 6{\cdot}34 + 0{\cdot}56\kappa$ (Houlsby & Martin, 2003) |
| Empirical factor | $D_F$ | Distribution factor: Defined as the ratio of the normal effective stress at the slip surface to the mean vertical effective stress within the sand frustum | For spudcan use equation (6): $D_F(\text{spudcan}) = 0{\cdot}642\left(\dfrac{H_s}{D}\right)^{-0{\cdot}576}$; $0{\cdot}16 \leq \dfrac{H_s}{D} \leq 1{\cdot}0$ For flat foundation use equation (7): $D_F(\text{flat}) = 0{\cdot}623\left(\dfrac{H_s}{D}\right)^{-0{\cdot}174}$; $0{\cdot}21 < \dfrac{H_s}{D} < 1{\cdot}12$ |

## IMPLEMENTATION OF THE $q_{peak}$ MODEL FOR CLAY–SAND–CLAY

### *Iterative procedure for estimating the operative friction and dilation angles*

The angles of friction and dilation: $\phi'$ and $\psi$ of sand can be related to each other using Bolton's equations (Bolton, 1986). Based on the work by Lee *et al.* (2013b), for the foundation peak resistance ($q_{peak}$), modified Bolton's equations are used taking the parameter $m$, which scales the relative dilatancy to determine the peak friction angle, as 2·65 so that

$$I_R = I_D\left(Q - \ln q_{peak}\right) - 1, \quad 0 \leq I_R \leq 4 \tag{23}$$

$$\phi' = \phi_{cv} + 2{\cdot}65 I_R \tag{24}$$

$$0{\cdot}8\psi = \phi' - \phi_{cv}, \quad \psi \leq 0 \tag{25}$$

Assuming that the in situ relative density, $I_D$, the natural logarithm of the grain crushing strength, $Q$ (in kPa; $Q \approx 10$ for siliceous sand), and critical state friction angle, $\phi_{cv}$, are known, an iterative solution procedure can be used to obtain $q_{peak}$, since $I_R$ is a function of $q_{peak}$. The iterative procedure can be performed by initially assuming an arbitrary value of $\psi$, allowing $\phi'$ to be estimated using equation (25). Equations (17), (23), (24) and (25) are then applied iteratively in sequence to generate predictions for $q_{peak}$. After each iteration, the $q_{peak}$ prediction is fed back into the system of equations to generate new values for $\phi'$ and $\psi$. The process is repeated, until the input and output values of $q_{peak}$ converge. In this manner, the dependency of the operative friction and dilation angle on the failure stresses are incorporated into the analytical model. The iteration can easily be incorporated into the type of spreadsheet programmes commonly used to generate profiles of jack-up leg penetration resistance.

### *Summary of parameters required for $q_{peak}$ prediction*

All the parameters required to estimate $q_{peak}$ have clear physical meaning and can be obtained from routine site investigation or laboratory tests. A description of the required parameters is given in Table 1.

## PERFORMANCE OF THE EXTENDED $q_{peak}$ MODEL

The performance of the extended clay–sand–clay model for the peak resistance during punch-through is verified by 27 new centrifuge model test results (Ullah *et al.*, 2017). These tests were conducted on samples consisting of medium dense to dense sand ($I_D$ = 51–74%) interbedded in clay with strength increasing with depth. Details of the centrifuge modelling apparatus and techniques are reported in the companion paper (Ullah *et al.*, 2017). In addition, three model test responses in denser sand ($I_D$ = 89%) reported

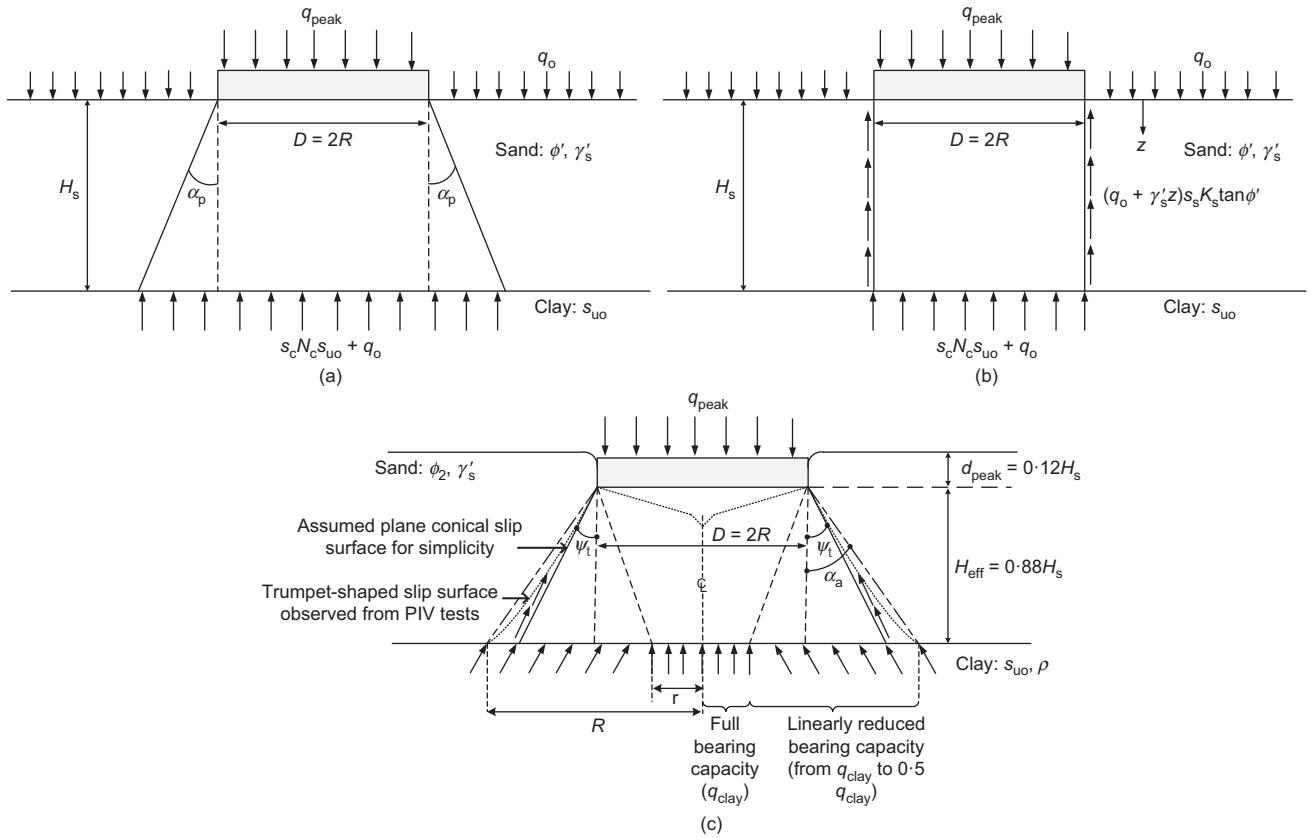


**Fig. 5. Schematic diagrams of: (a) the projected area (PA); (b) punching shear (PS); (c) Teh (2007) peak resistance mechanisms**

previously by Hossain (2014) have also been included in verification.

Moreover, the $q_{peak}$ prediction using the extended model is compared to the guidelines documented in ISO (2012), where the projected area (also known as load-spread) and the punching-shear methods are recommended (see Fig. 5). Some ambiguity exists in the ISO guidelines as to whether the weight of the sand frustum should be considered when calculating the surcharge term in the formulae for both methods (Hu *et al.*, 2015a). Thus, in the comparisons shown in Fig. 6, cases are presented which include (solid markers) and exclude (hollow markers) the weight of the sand frustum ($W_{SF}$) in the surcharge term. The effect of the additional top clay height ($H_{ct}$) was considered by replacing the surcharge term $q_o$ with the product of the clay layer height and its effective unit weight of $H_{ct}\gamma'_{ct}$.

The punch-through method of Teh (2007) is recommended as an alternative calculation method for sand–clay stratigraphies in ISO (2012) (see also Fig. 5(c)). To account for the additional top clay layer ($H_{ct}$) the peak bearing capacity ($q_{peak}$) equation of Teh (2007) has been extended (for which a full derivation is documented in the Appendix) as where the first term represents the clay bearing capacity, the second term represents the sand shear resistance and the third term is the effective sand frustum weight. $R$, $r$ and $\psi_t$ are geometric parameters and $\phi_2$ is the mean of operative and constant volume friction angle, that is $(\phi' + \phi_{cv})/2$, while $d_{peak}$ is taken as $0{\cdot}12H_s$.

The effect of $H_{ct}$ is to augment the peak capacity by increasing the sand shearing resistance and the bottom clay bearing capacity. If the top clay layer thickness, $H_{ct}$, is set to zero, the above equation reduces to that of Teh (2007) for sand–clay stratigraphies.

With the available centrifuge test results, Fig. 6 depicts the performances of the industry guidelines (Figs 6(a)–6(d)) (projected-area and punching-shear models), the Teh (2007) model extended with surcharge (Fig. 6(e)) and the three-layer clay–sand–clay model developed in this paper (Fig. 6(f)). The projected-area and punching-shear approaches of ISO (2012) are highly conservative, significantly under-predicting $q_{peak}$ (Figs 6(a)–6(d)). Excluding the weight of the sand frustum (hollow markers in Fig. 6) makes the prediction of $q_{peak}$ closer to the test data. The Teh (2007) model with extension to three layers performs better than both the projected-area

$$q_{peak}\frac{\pi D^2}{4} = \pi(N_{co}s_{ubi} + H_s\gamma'_s + H_{ct}\gamma'_{ct})\left[R^2 - \frac{0{\cdot}5}{R-r}\left(\frac{2}{3}R^3 + \frac{1}{3}r^3 - R^2r\right)\right] + \frac{\pi\gamma'_sK_p\sin(\varphi_2 - \psi_t)}{\cos\varphi_2\cos\psi}\left[\left(d_{peak} + \frac{1}{2}H_{eff}\right)DH_{eff} + d_{peak}\tan\psi_tH_{eff}^2 + \frac{2}{3}\tan\psi_tH_{eff}^3 + \frac{H_{ct}\gamma'_{ct}}{\gamma'_s}H_{eff}(\tan\psi_tH_{eff} + D)\right] - \frac{1}{3}\pi H_{eff}\left[\left(\frac{D}{2}\right)^2 + R\frac{D}{2} + R^2\right]\gamma'_s \quad (26)$$

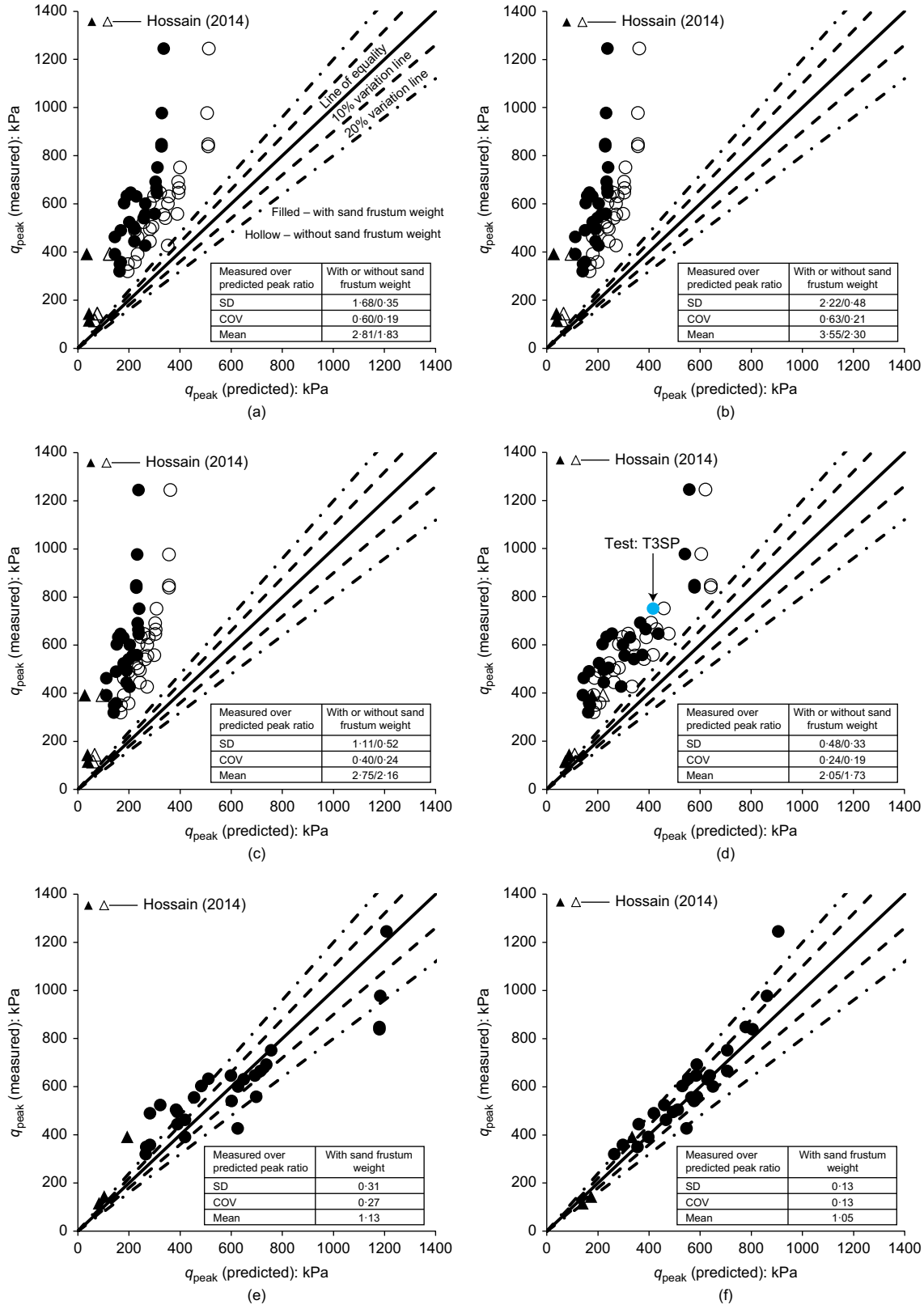


**Fig. 6. Observed performance in predicting the peak penetration resistance, $q_{peak}$: (a) projected area or load spread (1*h*:3*v*); (b) projected area or load spread (1*h*:5*v*); (c) punching shear approach (Sname, 2008); (d) punching shear approach (ISO, 2012); (e) extended Teh (2007) approach; (f) the proposed approach**

and punching-shear approaches (Fig. 6(e)). The three-layer clay–sand–clay model out-performs all of the other models, with most tests predicted within 20% variation bounds and the ratio of measured to predicted values of $q_{peak}$ very close to unity at 1·05 (Fig. 6(f)). In addition, the standard deviation (SD) and coefficient of variation (COV) of the predictions by the three-layer model are the lowest among all the models, indicating the reliability of the predictions.

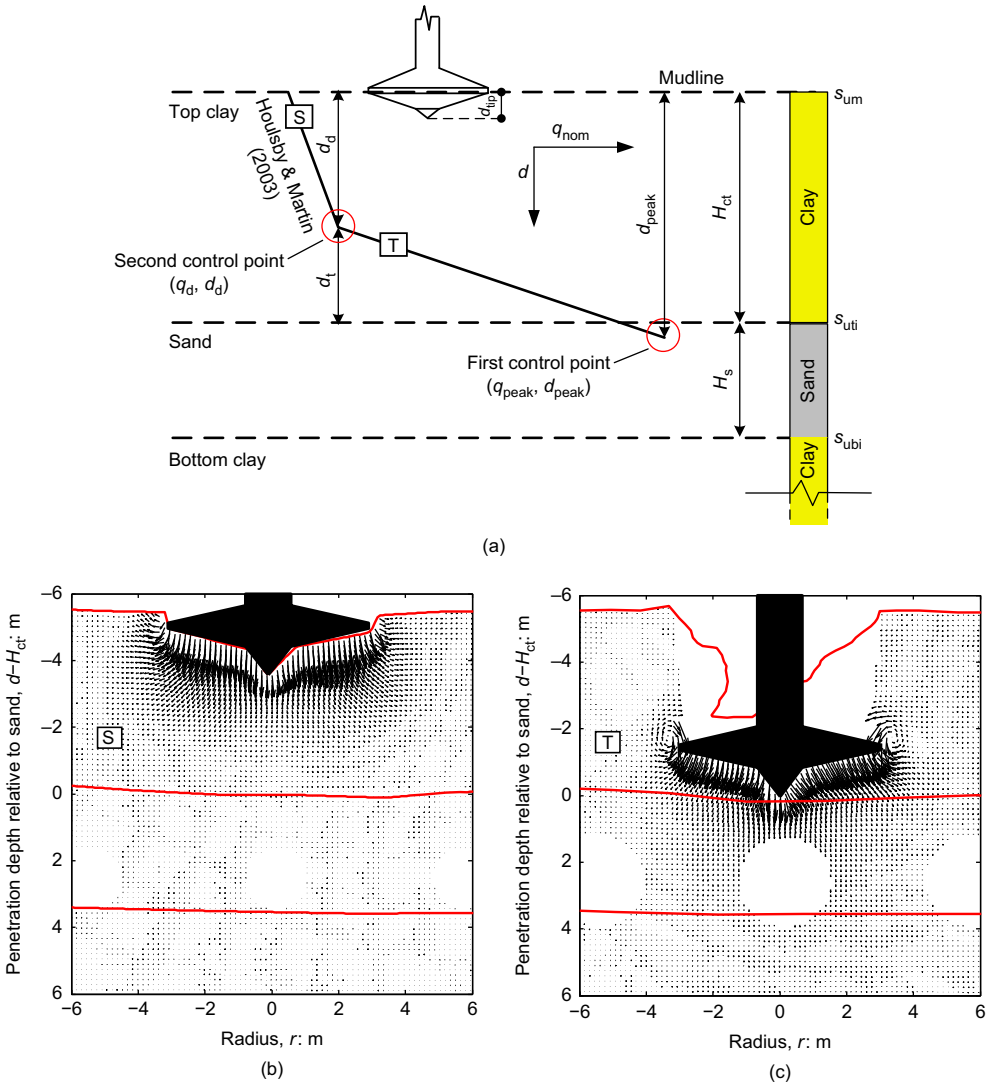


**Fig. 7. Top clay penetration resistance profile estimation: (a) diagram of key points in prediction; (b) soil flow mechanism prior to point of deviation; (c) soil flow mechanism after point of deviation**

## PREDICTION METHOD FOR PENETRATION RESISTANCE PROFILE

To ascertain the potential depth of punch-through failure ($d_{punch}$) in layered soils, a complete penetration resistance profile in all soil layers needs to be established. Thus, it is necessary to predict the resistance in the over- and underlying clay layers, especially the spudcan resistance in the underlying clay layer, in order to determine where the peak resistance can be recaptured.

### *Penetration resistance estimation in the top clay layer ($q_{clay\text{-}ct}$)*

The following equation is recommended to predict the resistance in the top clay layer

$$q_{clay-ct} = N_c s_u + q_o + \frac{4V_f}{\pi D^2}\gamma'_{ct} \quad (27)$$

The first term is the soil resistance, $q_o$ is the surcharge at the base of the foundation and the last term represents the buoyancy of the foundation in which $V_f$ is the volume of the foundation where $\gamma'_{ct}$ is the top clay effective unit weight. The bearing capacity factor $N_c$ in a single clay layer by Houlsby & Martin (2003) is adopted in equation (27).

By comparing the centrifuge test data and the $N_c$ factors by Houlsby & Martin (2003) in three-layer clay–sand–clay soils, Ullah *et al.* (2017) observed that at a certain depth in the upper clay layer the spudcan penetration resistance from the centrifuge test deviates from that predicted by the Houlsby & Martin (2003) solution (as point ($q_d$, $d_d$) in Fig. 7(a)). This depth is defined as the depth of deviation $d_d$. Beyond the deviation depth $d_d$, a transition takes place until the peak resistance is reached. During the transition, the spudcan resistance changes from the top clay mechanism (Fig. 7(b)) to the peak resistance mechanism (Fig. 7(c)). As the mobilisation of the sand layer generates a large increment in spudcan resistance over a relatively short penetration depth, the spudcan bearing capacity increases sharply and almost linearly (Fig. 1(b)).

The industry guidelines provided by ISO (2012) suggest that squeezing (characterised by significant lateral displacement of soils) will occur in a soft layer when a foundation is in close proximity to an underlying stiff layer. In the guidelines the onset of squeezing is defined by the following criterion

$$D \geq 3{\cdot}45(H_{ct}-d)\left(1+1{\cdot}025\frac{d}{D}\right) \quad \text{for } \frac{d}{D} \leq 2{\cdot}5 \quad (28)$$

When the criterion is satisfied, squeezing is assumed to occur and the penetration resistance is estimated after Meyerhof & Chaplin (1953) rather than using conventional bearing capacity theory.

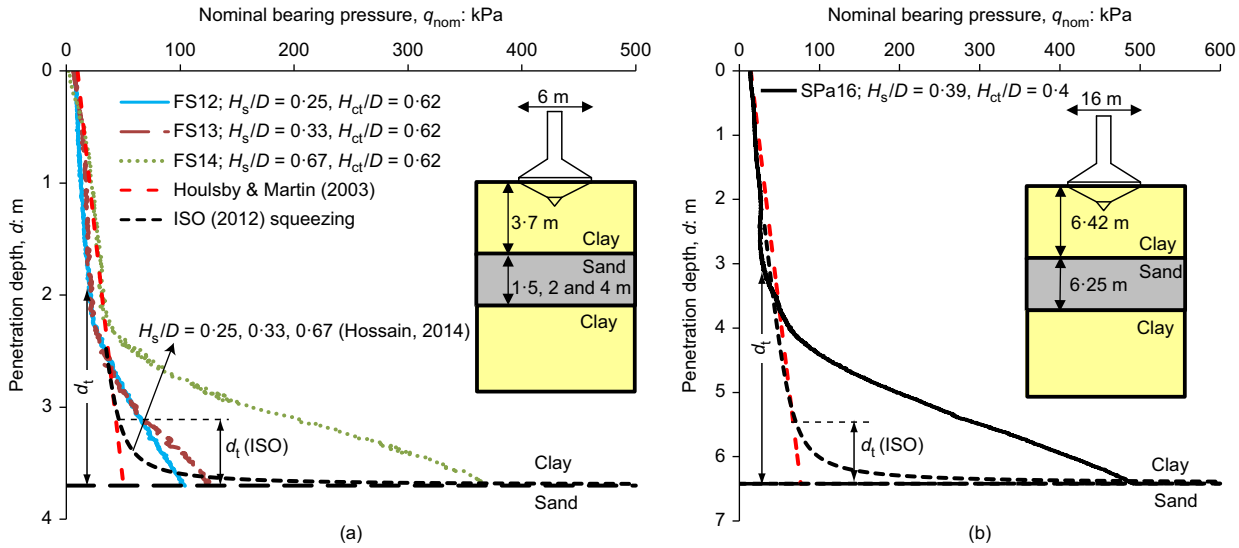


**Fig. 8. Comparison of ISO (2012) squeezing solution with centrifuge experiments from: (a) Hossain (2014); (b) Ullah *et al.* (2017)**

To examine the squeezing mechanism, Fig. 8(a) presents the comparisons between centrifuge test results for clay–sand–clay soils by Hossain (2014) (the arrow indicates the tests with increasing $H_s/D$) and the squeezing solution by ISO (2012), together with the solution for a single clay layer (Houlsby & Martin, 2003).

In the centrifuge tests the geometry and properties of the top clay layer were identical ($H_{ct}/D = 0{\cdot}62$, $s_{um} = 0{\cdot}5$ kPa and $\rho_{ct} = 0{\cdot}75$ kPa/m), and the sand layer had the same relative density of $I_D = 89\%$, but varying sand layer thickness ratio of $H_s/D = 0{\cdot}25$ to $0{\cdot}67$. It is clear that the squeezing solution from ISO (2012) is independent from the sand layer stiffness (i.e. sand $I_D$ and $H_s/D$) and the centrifuge test results show otherwise. At the same time, the depth of deviation $d_d$ is dependent on the sand layer stiffness as well. Similar results are obtained for the spudcan test in Fig. 8(b) (test SPa16 reported by Ullah *et al.* (2017)).

The influence of the underlying stiff layer on the penetration resistance has also been investigated in cone penetration tests (CPTs). Numerical analyses and field test data have shown that the strength and stiffness of underlying layers have an effect on the resistance in overlying layers (Van Den Berg *et al.*, 1996; Lunne *et al.*, 1997; Ahmadi & Robertson, 2005). The comparisons in Fig. 8 suggest that the geometry, strength and/or stiffness of the underlying layer have impacts on the depth of deviation $d_d$ from the bearing capacity solutions for jack-up foundations in the top clay layer as a single layer.

To address the above shortcomings of equation (28), an empirical formula is proposed below to predict the depth of transition, $d_t$

$$\frac{d_t}{D} = 0{\cdot}11\frac{H_{ct}}{D} + 0{\cdot}77\sqrt{\frac{H_s}{D}\left(\frac{\phi' - \phi_{cv}}{\phi_{cv}}\right)};$$
$$\frac{d_{tip}}{D} \le \frac{d_t}{D} \le \text{Min}\left[\left(\frac{H_{ct}}{D}\right), 0{\cdot}70\right] \qquad (29)$$

The first term approximates the effect of the top clay layer geometry, whereas the second term approximates the effect of the sand layer geometry and strength properties. The expression in equation (29) was calibrated using the centrifuge test data for sand layers with three relative densities of $I_D = 51\%$, 74% and 89%. The operative friction angle $\phi'$ can be obtained from the iterative peak resistance calculations (equations (17) and (23)–(25)). Hence, the stress-dependent characteristic of sand is taken into account.

The lower bound on $d_t/D$ in equation (29) is to ensure that the spudcan can sense the underlying sand layer as soon as the tip touches the sand. The upper bound is to ensure that $d_t/D$ does not exceed $H_{ct}/D$ and the maximum value of 0·70 for a rigid boundary. The maximum value of $d_t/D = 0{\cdot}70$ was derived using LDFE (large-deformation finite-element) analyses in Ullah *et al.* (2014) and agrees well with the solution of $\sim 0{\cdot}71$ by Mandel & Salencon (1969), using the method of characteristics.

A graphical representation of equation (29) is displayed in Fig. 9 for $H_s/D = 0{\cdot}75$. The effects of clay and sand layer geometry and sand strength properties on $d_t/D$ are illustrated for a spudcan with $d_{tip}/D = 0{\cdot}23$ (typical of Marathon Le Tourneau spudcan widely modelled at the University of Western Australia (UWA); see Menzies & Roper (2008) for an illustration of the geometry) and a flat foundation (where $d_{tip}/D = 0$). In general, $d_t$ increases with increasing $H_{ct}/D$ and $(\phi' - \phi_{cv})/\phi_{cv}$. The range of $d_t$ is greater for a flat footing than for a spudcan with conical underside owing to the bounds in equation (29).

After $d_t$ is estimated, the depth of deviation from the mudline $d_d$ can be calculated as

$$d_d = H_{ct} - d_t \ge 0 \qquad (30)$$

The performance verification of equation (30) can be found later in the section where the spudcan full penetration profiles from centrifuge tests and from the proposed framework predictions are compared.

Once the peak resistance ($q_{peak}$), depth of peak resistance ($d_{peak}$) and depth of deviation ($d_d$) have been calculated, the penetration resistance profile in the top clay layer ($q_{clay\text{-}ct}$) can be estimated as follows.

(*a*) Calculate the penetration resistance profile in the top clay layer ($q_{clay\text{-}ct}$) over the range of $0 \le d \le d_d$ using equation (27) with $N_c$ from Houlsby & Martin (2003).
(*b*) Construct a straight line between the penetration resistance at deviation $q_d$ (which occurs at the depth of deviation $d_d$) to the peak resistance $q_{peak}$ (which occurs at the depth of peak resistance $d_{peak}$).

This procedure is much simpler than that of the squeezing mechanism suggested by ISO (2012). At the same time, it provides better predictions of spudcan penetration resistance when compared with centrifuge data. More demonstrations

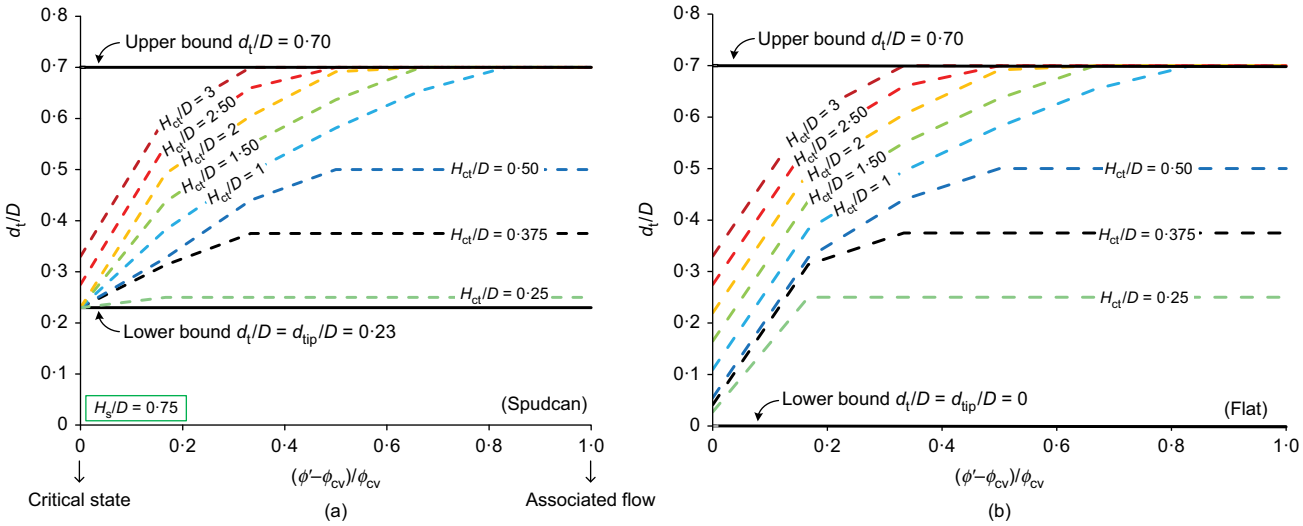


**Fig. 9. Nomogram of the depth of transition for $H_s/D$ of 0·75: (a) a typical spudcan with spigot (or tip); (b) a flat foundation**

of comparison can be found later in the full penetration profile section.

*Penetration resistance estimation in the bottom clay layer ($q_{clay\text{-}cb}$)*

The centrifuge experiments of Ullah *et al.* (2017) used image analysis to reveal that a small clay plug and a substantial sand plug become entrapped beneath jack-up footings following penetration through the sand layer (see Ullah *et al.*, 2017). The proportion of the entrapped plug that consisted of sand was very similar in size to that entrapped beneath similar foundations in two-layer sand–clay punch-through failure experiments reported by both Teh *et al.* (2008) and Hu *et al.* (2014b), with an average height of $0{\cdot}9H_s/D$. Therefore, the following formula is proposed to estimate the height of the composite plug $H_{plug}$ for clay–sand–clay stratigraphies as

$$H_{plug} = 0{\cdot}9H_s + H_c \tag{31}$$

where $H_c$ is as defined earlier at $0{\cdot}07H_{ct}$. The height of the composite foundation $H_{fdn}$ is then expressed as

$$H_{fdn} = H_{plug} + t \tag{32}$$

where $t$ is the thickness of the foundation. For a spudcan, $t$ is the thickness of the shoulder.

The resistance in the bottom clay layer is then expressed as

$$q_{clay-cb} = N_c s_u + H_{fdn}\gamma'_{cb} \tag{33}$$

The first term represents the resistance from the soil, whereas the second term represents the buoyancy of the displaced soil. $N_c$ is the deep bearing capacity factor, $s_u$ is the undrained shear strength at the load reference point (LRP) on the foundation and $\gamma'_{cb}$ is the effective unit weight of the bottom clay layer.

The following semi-empirical expression for $N_c$ (calibrated from measured resistances at $0{\cdot}5D$ penetration into the bottom clay layer) in the underlying clay layer in clay–sand–clay stratigraphies is proposed

$$N_c = 0{\cdot}55\frac{H_{ct}}{D} + 11\frac{H_s}{D} + 10{\cdot}5 \tag{34}$$

The $N_c$ factor is strongly proportional to the $H_s/D$ ratio and slightly augmented by the $H_{ct}/D$ ratio because the sand layer provides a greater proportion of the entrapped plug volume than the upper clay layer. For a purely sand over clay case (where $H_{ct}/D = 0$), equation (34) simplifies to that proposed by Hu *et al.* (2015c) for sand–clay stratigraphies, thus like the $q_{peak}$ model proposed earlier in this paper, the penetration resistance in the underlying clay can be evaluated for both clay–sand–clay as well as sand–clay stratigraphies using equations (33) and (34) by setting $H_{ct}/D = 0$ where appropriate.

Hu *et al.* (2015c) found that the sand relative density ($I_D = 43$–$99\%$) and the angle of the underside of the spudcan ($\theta_b = 0$–$21°$) has no systematic impact on $N_c$ for sand–clay stratigraphies and similarly no significant trends were observed in the experiments reported by Ullah *et al.* (2017) for clay–sand–clay stratigraphies. To account for potential variability of soil properties with depth, it was recommended by Hu *et al.* (2015c) that $N_c \pm 1\sigma$ be used to generate upper and lower bounds on the penetration resistance in the underlying clay layer from the best estimate soil strength, where $\sigma$ is the SD from the mean $N_c$, which for the experiments reported here is 1·73.

*Summary of the full penetration resistance profile prediction method*

A simplified prediction model for the full penetration resistance profile of spudcan on clay–sand–clay stratigraphies can be idealised by four linear segments, as illustrated schematically in Fig. 10. The flow chart in Fig. 11 outlines the calculations required to generate an estimate of the full penetration resistance profile illustrated in Fig. 10.

This prediction method follows neither the 'top-down' approach nor 'bottom-up' approaches recommended in the industry guidelines (ISO, 2012) because the operative friction of the sand layer at peak resistances contributes to both the peak penetration resistance ($q_{peak}$) and penetration resistance in the top clay layer ($q_{clay\text{-}ct}$), so the peak resistance must be calculated first. The four calculation points capture the key parameters in a punch-through assessment – the peak resistance (which should not be exceeded by the leg load if the punch-through distance is unacceptably large) and the punch-through distance.

For sand–clay stratigraphies the penetration profile prediction approach is identical except that the top clay layer height $H_{ct}$ is set to zero and the coordinate ($q_{peak}$, $d_{peak}$) is connected to the coordinate (0, $-d_{spg}$), where $d_{spg}$ is the height of the spigot (i.e. $d_{spg}$ is 0 for a flat foundation).

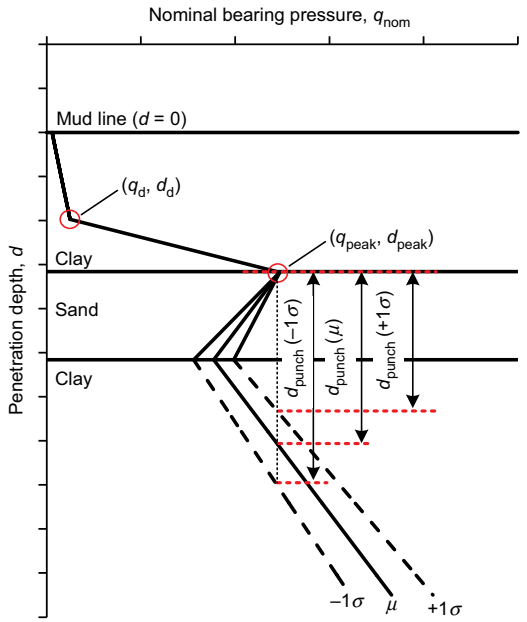


**Fig. 10. Schematic representation of the proposed full penetration resistance profile prediction method**

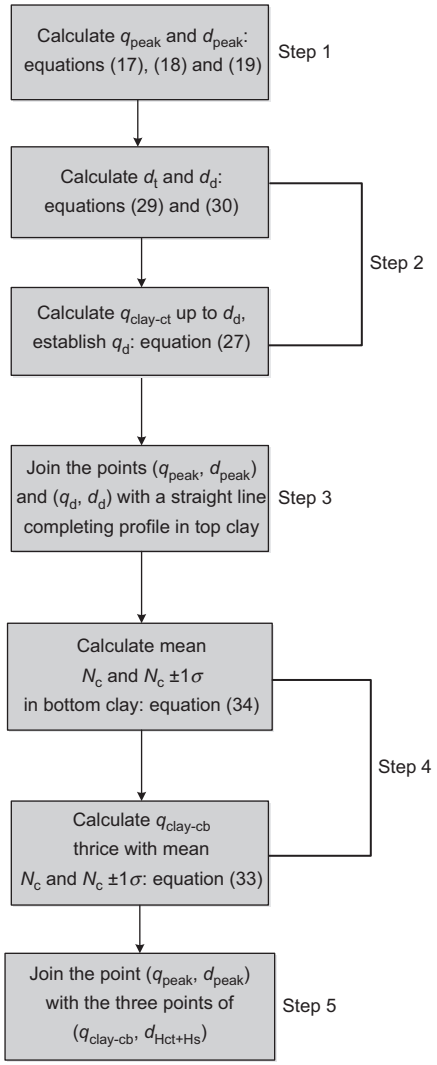


**Fig. 11. Flow chart for full penetration resistance profile prediction**

## PERFORMANCE OF FULL RESISTANCE PROFILE MODEL

Figure 12 demonstrates the performance of the model in predicting the penetration resistance measured in three selected centrifuge experiments modelling punch-through of jack-up foundations: two for clay–sand–clay with dense and medium dense sand layers and one for dense sand overlying clay.

Solutions generated using the ISO (2012) recommendations are shown alongside. The punching-shear approach was used to predict the peak resistance, $q_{peak}$. The penetration resistance in the top clay was calculated using the relations provided in Houlsby & Martin (2003) in conjunction with the squeezing model of Meyerhof & Chaplin (1953) when the criterion in equation (28) was satisfied. The penetration resistance in the bottom clay layer was also estimated using $N_c$ values after Houlsby & Martin (2003), thereby ignoring the presence of the entrapped plug of soil beneath the foundation as the ISO (2012) recommendations make no specific provision to account for any entrapped material beneath the foundation following punch-through.

A number of observations are drawn from these three comparisons.

(*a*) The ISO (2012) calculations under-predict the penetration resistance, both in the prediction of $q_{peak}$ and $q_{clay-cb}$, which fortuitously results in quite acceptable predictions for the potential punch-through depth, $d_{punch}$ (see for instance Fig. 12(a) test T3SP, which is marked with an arrow in Figs 6, 13 and 14 to highlight this phenomenon).

(*b*) The proposed approach yields similar predictions for the potential punch-through depth, $d_{punch}$, but as a product of much more accurate predictions of $q_{peak}$ and $q_{clay-cb}$ than the ISO (2012) calculations, providing confidence in the various stages of the penetration resistance profile calculation. This greater accuracy raises the predicted maximum tolerable leg load without causing punch-through, compared to the ISO method.

(*c*) The linear simplifications employed by the model to approximate the transitions from $q_{peak}$ to $q_{clay-cb}$ tend to underestimate the penetration resistance during punch-through. This is desirable as it provides a worst-case interpretation of the penetration resistance profile during punch-through. A more detailed increment-by-increment assessment could be performed using the same methodology, leading to a modest increase in realism.

(*d*) The performance of the model for sand–clay stratigraphies is comparable to that for clay–sand–clay stratigraphies. This was expected because when $H_{ct} = 0$, the penetration resistance profile model simplifies to the sand–clay model proposed and verified – both experimentally and numerically – by Hu *et al.* (2015b, 2015c).

Performance assessments for all the tests of Ullah *et al.* (2017) are available in the supplementary data.

Figure 13 presents a comparison of the value of $N_c$ measured (by dividing the net penetration resistance $q_{net}$ by the strength at that depth measured using a T-bar; see Ullah *et al.* (2017)) and back-calculated using equation (33) at the depth at which $q_{clay-cb}$ was equal to $q_{peak}$ for each experiment (i.e. the depth at which punch-through failure would cease). The industrial guidelines of ISO (2012) and Sname (2008) consistently under-predict $N_c$ in the bottom clay layer because they do not account for soil plug entrapment, which has been observed in image analysis (Ullah *et al.*, 2017).

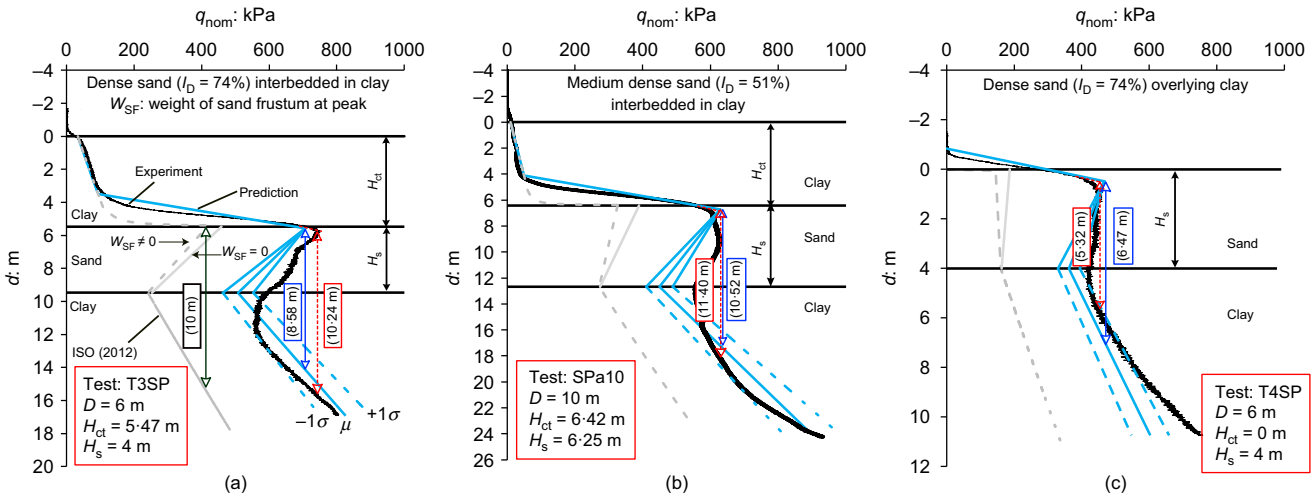


**Fig. 12. Prediction of complete penetration resistance profile on: (a) clay–sand–clay with a dense sand layer; (b) clay–sand–clay with a medium dense sand layer; (c) dense sand overlying clay**

Two variants of $N_c$, one explicitly neglecting and one considering additional shear resistance along the trapped plug, was considered in the extended method of Teh (2007) (Fig. 13(e)), given in equations (35) and (37), respectively

$$N_c = \frac{(q_{clay-cb} - 4V_f/\pi D^2 \gamma'_{cb})}{s_{u(base)}} \quad (35)$$

where $s_{u(base)}$ is the undrained shear strength at the base of the soil plug and $q_{clay-cb}$ as in Teh (2007) is given as

$$q_{clay-cb} = N_c s_{u(base)} + \frac{4 s_{ua} \alpha_{side} H_{fdn}}{D} + \frac{4V_f}{\pi D^2} \gamma'_{cb} \quad (36)$$

where $s_{ua}$ is the average strength within the depth of the soil plug, $\alpha_{side}$ represents the side sand–clay interface adhesion factor assumed as unity and $N_c$ is adopted from Hossain *et al.* (2006)

$$N_c = 10\left(1 + 0{\cdot}075\frac{d + H_{plug}}{D}\right) \leq 11{\cdot}5 \quad (37)$$

The extended approach by Teh (2007) similarly does not capture the range in $N_c$ measured due to the volume of soil entrapment beneath the foundation. In contrast, the proposed approach performs reasonably well in predicting the experimental measurements with no systematic bias evident. Although the measurements are somewhat scattered about the mean, both the SD and COV are lower than the other methods.

Figure 14 presents a comparison of the measured and predicted punch-through depth $d_{punch}$ for each of the experiments. Somewhat surprisingly, the industrial guidelines generate very good predictions for $d_{punch}$; however, it should be stressed that this is fortuitously a product of conservative predictions for both $q_{peak}$ and $q_{clay-cb}$.

The extended version of the Teh (2007) approach performs better than the ISO (2012) approaches. However, ~26% of the predictions indicated no risk of punch-through even though punch-through occurred in the experiments and there is significant scatter in the predictions, as reflected by the mean, SD and COV of predicted over measured $d_{punch}$ ratio (Fig. 14(e)). By correctly modelling stress dependency of the sand layer in $q_{peak}$ calculations and by considering the enhancement of $N_c$ (due to soil plug entrapment) in the underlying clay layer, excellent predictions of $d_{punch}$ can be obtained. The majority of the tests predict $d_{punch}$ with values mostly within ±25% variation, with a mean predicted over measured $d_{punch}$ ratio of unity and relatively low SD and COV (Fig. 14(f)).

The performance of the proposed approach has been verified by comparison of the predictions to measurements from 30 centrifuge model tests. The comparisons indicate that the proposed approach is superior to adaptations of the industry guidelines and other models for clay–sand–clay scenarios. The approach is simple and formulated in terms of meaningful physical parameters that can be defined by performing standard in situ tests, making the model well suited for performing routine punch-through assessment for locations with clay–sand–clay or sand–clay stratigraphies.

## CONCLUSIONS

An analytical approach has been proposed to allow routine assessment of punch-through risk for jack-up rig foundations in clay–sand–clay stratigraphies. The method allows the spudcan peak resistance and the potential punch-through depth to be estimated more accurately. The method extended the current failure stress-dependent models for sand–clay stratigraphies (Lee *et al.*, 2013b; Hu *et al.*, 2014a) to three-layer clay–sand–clay soils. The model proposed was validated against 30 centrifuge model test results. The model performance was compared with those generated by interpretations of the current industry guidelines (ISO, 2012). The following conclusions are obtained.

(*a*) An extension of the failure stress-dependent model for the peak penetration resistance $q_{peak}$ in the sand layer during punch-through for sand–clay stratigraphies (see Lee *et al.*, 2013b; Hu *et al.*, 2014a) has resulted in a universal model for $q_{peak}$ that is suitable for generating predictions for both sand–clay and clay–sand–clay scenarios. The extended model performs very well in predicting $q_{peak}$ for both sand–clay and clay–sand–clay cases for the geometries and soil properties tested in this pair of companion papers. There is less bias and scatter than the other methods considered in the performance comparison.

(*b*) Similarly, a very simple semi-empirical extension of the bearing capacity model for the underlying clay layer following punch-through (Hu *et al.*, 2014b) has been proposed that performs equally well for sand–clay or clay–sand–clay scenarios, for the geometries and soil properties tested in this pair of companion papers.

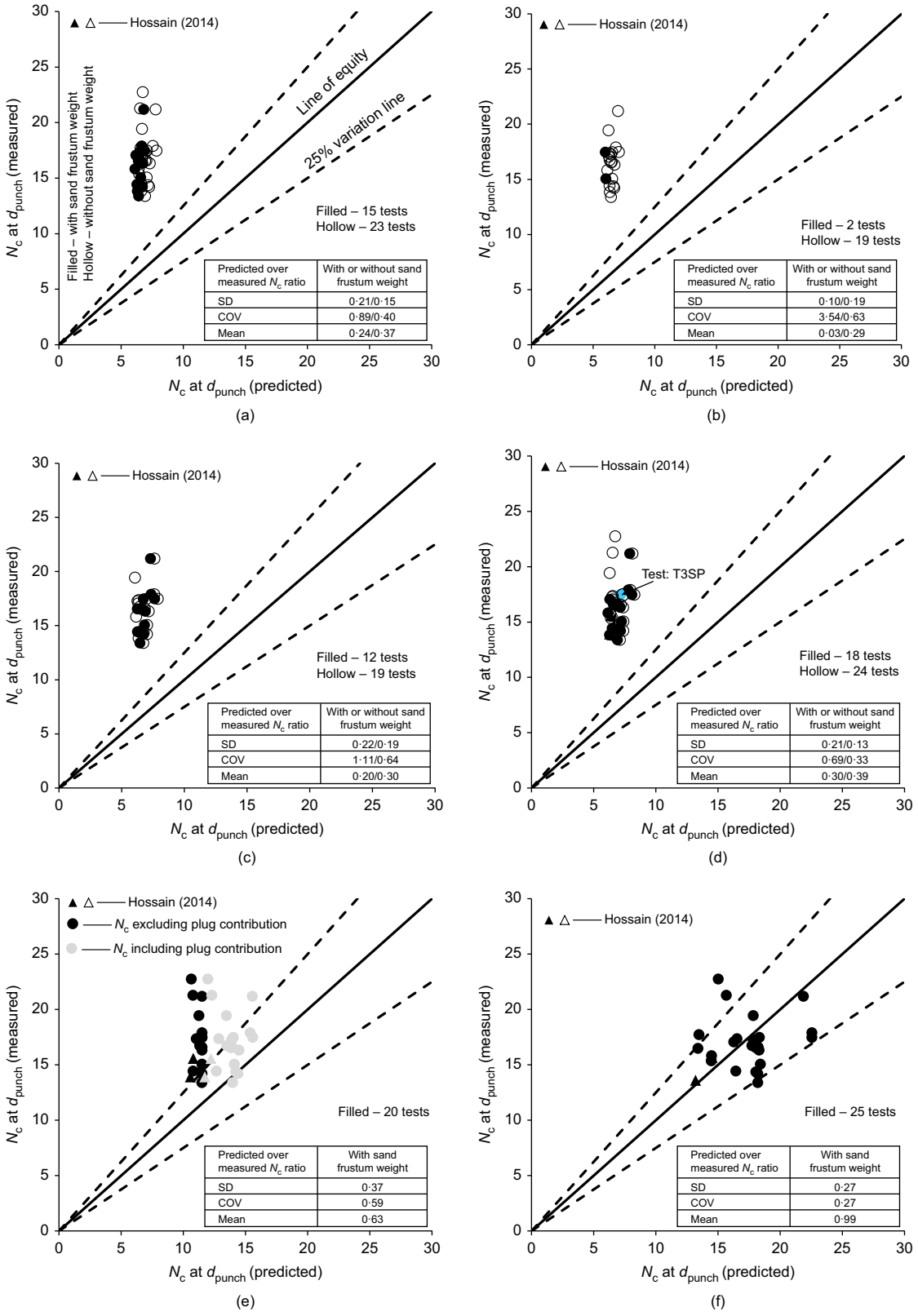


**Fig. 13. Predicted plotted against measured back-calculated bearing capacity factor ($N_c$) in the underlying clay layer: (a) projected-area or load-spread (1*h*:3*v*); (b) projected-area or load-spread (1*h*:5*v*); (c) punching-shear approach (Sname, 2008); (d) punching shear approach (ISO, 2012); (e) extended Teh's approach (Teh, 2007); (f) proposed approach**

Prediction of the penetration resistance in the underlying clay layer $q_{clay}$ and the peak resistance $q_{peak}$ allows the potential punch-through depth to be estimated. The proposed approach implicitly accounts for the change in bearing capacity factor mobilised for different entrapped soil plug geometries; a feature that is not captured by current industry guidelines.

(*c*) The combination of the calculations referred to in 1 and 2 above results in good predictions of the punch-through depth $d_{punch}$. Critically, the proposed method captures more accurately the punch-through

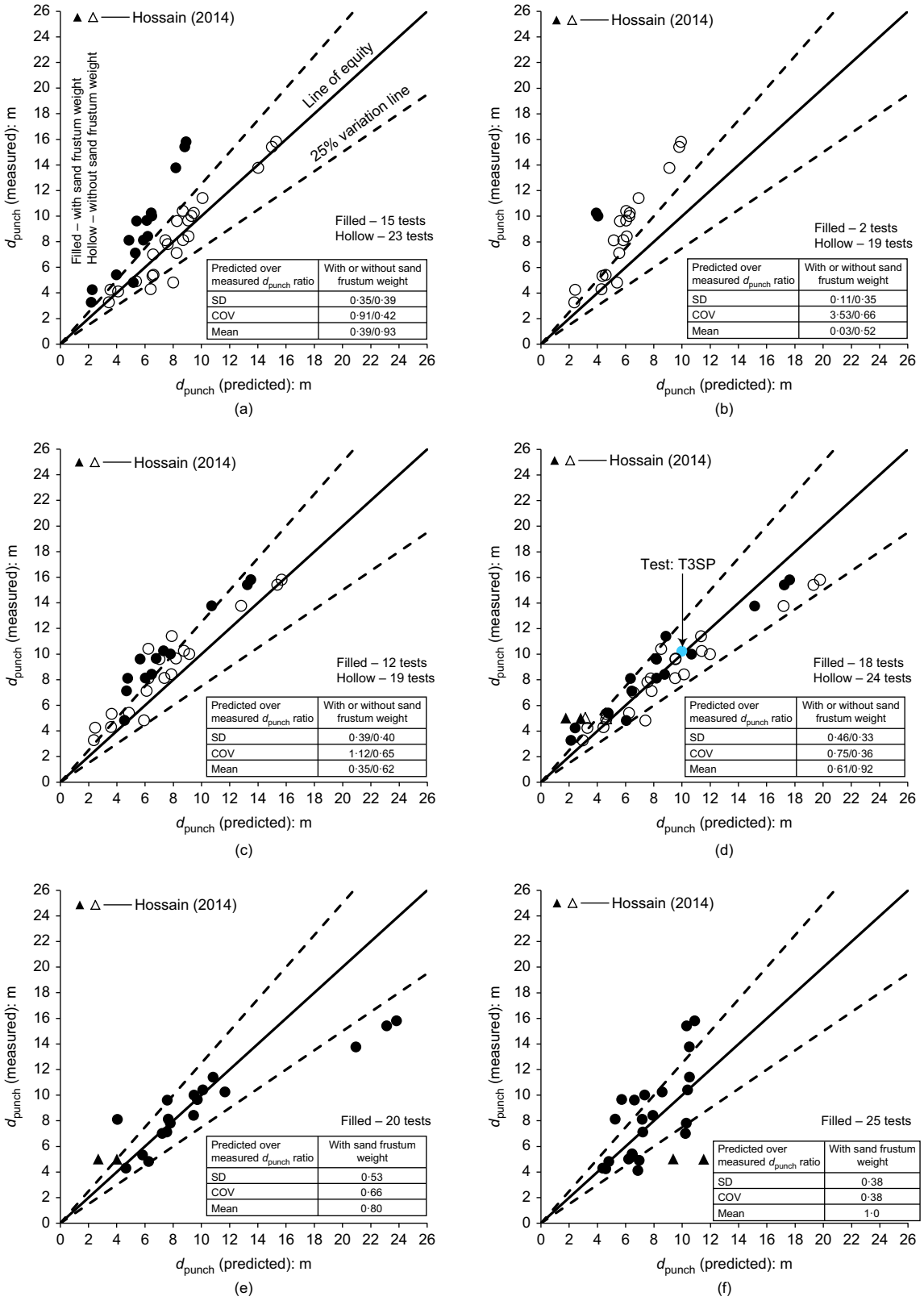


**Fig. 14. Performance in terms of predicting punch-through depth, $d_{punch}$: (a) projected-area or load-spread (1*h*:3*v*); (b) projected-area or load-spread (1*h*:5*v*); (c) punching-shear approach (Sname, 2008); (d) punching-shear approach (ISO, 2012); (e) extended Teh's approach (Teh, 2007); (f) proposed approach**

risk than the current industry guidelines or alternative recommendations, as well as being more accurate in predicting $q_{peak}$, thus raising the allowable leg load range for the conditions considered in this study.

(*d*) The penetration resistance preceding peak resistance has been approximated using an alternative semi-empirical approach to the squeezing model recommended in the industry guidelines. This model accounts for the geometry of the layers and their strength, leading to more accurate estimation of the depth of transition from classical shallow bearing capacity to punch-though failure than current industry

recommendations. In addition, this relation is appropriately bounded to account for spudcan underside geometry leading to early sensing of the stiff underlying boundary, which precludes 'squeezing-type' mechanisms.

(*e*) The models were developed with the aid of particle image velocimetry (PIV) observations derived from model tests using one spudcan and flat footing diameter (6 m in prototype terms) in medium dense to dense sand interbedded in clay (Ullah *et al.*, 2017). Although the models yield excellent predictions for foundations with prototype diameters in the range from 6 m to 16 m, there is potential for further refinement (particularly the fitting parameters $f_1$ and $f_2$, for example) in the future through further centrifuge tests, or ideally from field observations.

(*f*) The models developed can be applied to both clay–sand–clay and sand–clay stratigraphies. All steps are expressed analytically, making the approach easily coded into a spreadsheet or other software for routine use.

(*g*) All the parameters required to estimate the penetration resistance profile have clear physical meaning and can be obtained from existing laboratory tests.

## ACKNOWLEDGEMENTS

The research presented here forms part of the activities of the Centre for Offshore Foundation Systems (COFS), currently supported as a node of the Australian Research Council Centre of Excellence for Geotechnical Science and Engineering (grant CE110001009) and through the Fugro Chair in Geotechnics, the Lloyd's Register Foundation Chair and Centre of Excellence in Offshore Foundations and the Shell EMI Chair in Offshore Engineering (held by the fourth author). The authors would like to acknowledge the financial contribution of the Australian Research Council (ARC) through Discovery Project DP1096764.

## APPENDIX. EXTENDED TEH METHOD

The method of Teh (2007) is strictly applicable to sand over clay soils only, as no surcharge ($q_o$) term was considered while developing the model. However, for comparison purposes, the method is extended here to incorporate the effective surcharge ($q_o = H_{ct}\gamma'_{ct}$) as follows.

According to Teh (2007), the foundation peak resisting force ($Q$) from soil is given as

$$Q = Q_s + Q_c - W \tag{38}$$

where $Q_s$ is the sand shearing resistance, $Q_c$ is the resistance contribution from the bottom clay and $W$ is the weight of the sand frustum. The effect of the additional surcharge is to increase the sand shearing resistance and the bottom clay bearing capacity. The weight of the sand frustum is unaffected by the presence of the surcharge $q_o$. The contributions of $q_o$ on $Q_s$ and $Q_c$ are evaluated separately below.

### *Evaluating the sand shearing resistance, $Q_s$*

Referring to Fig. 15, Teh (2007) assumed that the stresses at the side of the sand frustum are in a passive state. Hence, if $N$ is the total normal force acting on the side of the frustum and $A_{ls}$ is the lateral surface area of the sand frustum, then the Rankine's effective passive earth pressure $\sigma'_{hp}$ can be written as

$$\sigma'_{hp} = \frac{dN}{dA_{ls}} = \gamma'_s K_p (d_{crit} + z) + q_o K_p \tag{39}$$

where $K_p$ is the Rankine's passive earth pressure coefficient given as

$$K_p = \frac{1 + \sin\phi'}{1 - \sin\phi'} \tag{40}$$

where $\phi'$ is the operative friction angle calculated through an iterative procedure by way of Bolton's strength–dilatancy relationships (Bolton, 1986).

Next, $A_{ls}$ is expressed as

$$A_{ls} = \frac{\pi z}{\cos\psi}(z\tan\psi_t + D) \tag{41}$$

Therefore, $dA_{ls}/dz$ can be written as

$$\frac{dA_{ls}}{dz} = \frac{\pi}{\cos\psi_t}(2z\tan\psi_t + D) \tag{42}$$

Next, using the chain rule

$$\frac{dN}{dz} = \frac{dN}{dA_{ls}} \times \frac{dA_{ls}}{dz} = \frac{\pi K_p \gamma'_s}{\cos\psi}\left[(d_{crit} + z)D + 2z\tan\psi d_{crit} + 2z^2\tan\psi + \frac{q_o}{\gamma'_s}(2z\tan\psi + D)\right] \tag{43}$$

The above equation can be integrated to give the total normal force on the slip plane $N$ as

$$\int_0^{H_{eff}} \frac{dN}{dz}\,dz = [N]_0^{H_{eff}} = \frac{\pi\gamma'_s K_p}{\cos\psi_t}\left[\left(d_{crit} + \frac{1}{2}H_{eff}\right)DH_{eff} + d_{crit}\tan\psi_t H_{eff}^2 + \frac{2}{3}\tan\psi_t H_{eff}^3 + \frac{q_o}{\gamma'_s}H_{eff}(\tan\psi_t H_{eff} + D)\right] \tag{44}$$

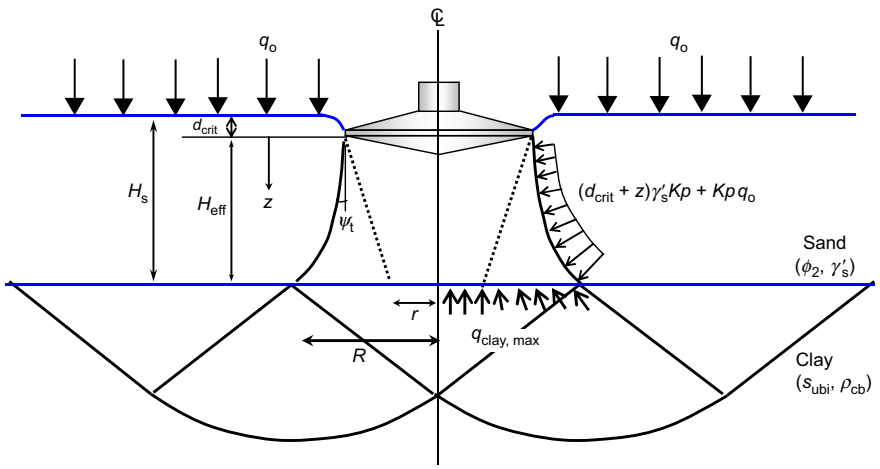


**Fig. 15. Extended Teh (2007) model with added surcharge $q_o$ (modified after Teh, 2007)**

The last term in the above equation contains the surcharge $q_o$. The effect of which is to augment the total normal force $N$ and therefore contribute to the sand shearing resistance.

As in the Teh (2007) method, the failure plane is a logarithmic spiral with the initial portion of this plane being inclined at an angle $\psi_t$ (see Figs 15 and 16; note that $T$ is the resultant force in Fig. 16). The vertical shear force in sand $Q_s$ can be evaluated as

$$Q_s = \frac{\pi\gamma'_s K_p \sin(\varphi_2 - \psi_t)}{\cos\varphi_2 \cos\psi_t}\left[\left(d_{crit} + \frac{1}{2}H_{eff}\right)DH_{eff} + d_{crit}\tan\psi_t H_{eff}^2 + \frac{2}{3}\tan\psi_t H_{eff}^3 + \frac{q_o}{\gamma'_s}H_{eff}(\tan\psi_t H_{eff} + D)\right] \quad (45)$$

where $\phi_2$ is defined as

$$\phi_2 = \frac{1}{2}(\phi' + \phi_{cv}) \quad (46)$$

which is the mean of the operative and critical state friction angle. If $q_o$ is assumed as zero in equation (45) above, the equation reduces to that of Teh (2007). Also, note that the term $\psi_t$ in this equation is not a dilatancy angle, but rather it is a geometric term representing the initial inclination of the logarithmic failure surface and depends on $H_s/D$ and $q_{clay}/q_{sand}$. Where $q_{sand}$ is the bearing capacity of a foundation resting on sand alone and is given by the following

$$q_{sand} = \frac{\gamma'_s D}{2}N_{\gamma,cone} + (\gamma'_s d + q_o)N_{q,cone} \quad (47)$$

where $d$ is the penetration depth corresponding peak with the bearing capacity factors $N_{\gamma,cone}$ and $N_{q,cone}$ defined in Teh (2007).

$q_{clay}$ is the bearing capacity of the clay layer and can be written as

$$q_{clay} = N_{co}s_{ubi} + q_o \quad (48)$$

where $N_{co}$ is taken from Houlsby & Martin (2003) as

$$N_{co} = 6{\cdot}34 + 0{\cdot}56\left(\frac{\rho_{cb}D}{s_{ubi}}\right) \quad (49)$$

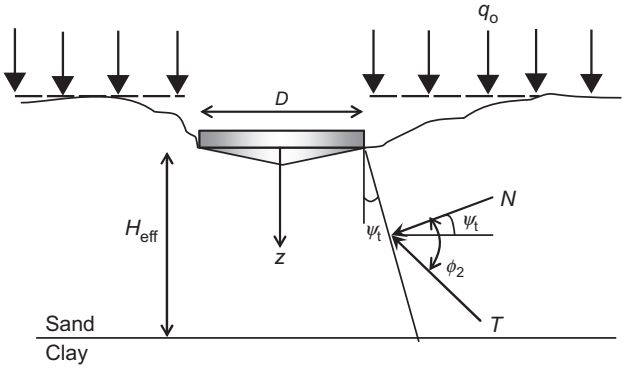


**Fig. 16. Simplified force diagram on sand failure surface; $N$ is the total normal force and $T$ is the resultant force (modified after Teh, 2007)**

*Evaluating the clay bearing force at peak, $Q_c$*

Considering the effect of the surcharge, $Q_c$ can be directly evaluated as

$$Q_c = \pi(N_{co}s_{ubi} + H_s\gamma'_s + q_o)\left[R^2 - \frac{0{\cdot}5}{R-r}\left(\frac{2}{3}R^3 + \frac{1}{3}r^3 - R^2 r\right)\right] \quad (50)$$

where $R$ and $r$ are geometric parameters obtained from charts provided in Teh (2007) which are introduced to take into account the reduction in vertical bearing capacity of clay due to the presence of inclined loading (Fig. 15). Notice that $Q_c$ reduces to that of Teh (2007) without surcharge.

The weight of the sand frustum ($W$) is not affected by the surcharge and can be written as

$$W = \frac{1}{3}\pi H_{eff}\left[\left(\frac{D}{2}\right)^2 + R\frac{D}{2} + R^2\right]\gamma'_s \quad (51)$$

Now $q_o$ can be expressed as products of the top clay height ($H_{ct}$) and the effective unit weight of top clay ($\gamma'_{ct}$).

Hence by putting the value of $q_o = H_{ct}\gamma'_{ct}$ to equations (8) and (13) the final equation for peak bearing force $Q$ from equation (1) can be rewritten as

$$\begin{aligned} Q =& \pi(N_{co}s_{ubi} + H_s\gamma'_s + H_{ct}\gamma'_{ct})\left[R^2 - \frac{0{\cdot}5}{R-r}\left(\frac{2}{3}R^3 + \frac{1}{3}r^3 - R^2 r\right)\right] \\ &+ \frac{\pi\gamma'_s K_p \sin(\phi_2 - \psi_t)}{\cos\phi_2\cos\psi_t}\left[\left(d_{crit} + \frac{1}{2}H_{eff}\right)DH_{eff} + d_{crit}\tan\psi_t H_{eff}^2 + \frac{2}{3}\tan\psi_t H_{eff}^3 + \frac{H_{ct}\gamma'_{ct}}{\gamma'_s}H_{eff}(\tan\psi_t H_{eff} + D)\right] \\ &- \frac{1}{3}\pi H_{eff}\left[\left(\frac{D}{2}\right)^2 + R\frac{D}{2} + R^2\right]\gamma'_s \end{aligned} \quad (52)$$

If the top clay layer thickness, $H_{ct}$ is set to zero, the above equation reduces to that of Teh (2007) for sand over clay soil without surcharge. This shows the consistency of the newly derived equation which is used to assess the performance of the Teh (2007) method against the three-layer tests.

*Calculating $\phi_2$ in modified Teh method*

$\phi_2$ was defined earlier in equation (46) as the average of the constant volume friction angle ($\phi_{cv}$) and the operative friction angle $\phi'$. In the iterative procedure involving Bolton's equations (Bolton, 1986) suggested by Teh (2007), the mean effective stress $p'_o$ needs to be calculated incorporating the additional vertical stresses from the top clay layer as follows

$$\begin{aligned} p'_o &= \frac{1}{2}\left[\left(H_{ct}\gamma'_{ct} + \frac{\gamma'_s H_s}{2}\right) + \left(H_{ct}\gamma'_{ct} + \frac{\gamma'_s H_s}{2}\right)K_p\right] \\ &= \frac{1}{4}\left[(2H_{ct}\gamma'_{ct} + \gamma'_s H_s)(1 + K_p)\right] \end{aligned} \quad (53)$$

$K_p$ is a function of $\phi'$ and was defined in equation (40). Hence, equation (53) can be used to arrive at an operative friction angle $\phi'$ taking the Bolton (1986) $m$ parameter to be equal to 3. $\phi'$ and $\phi_2$ can be evaluated from equation (46). As $\phi_{cv}$ is typically lower than $\phi'$, $\phi_2$ is usually smaller than $\phi'$.

## NOTATION

$A$ bearing area of circular foundation
$A_{ls}$ lateral surface area of sand frustum
$D$ foundation diameter

$D_F$ distribution factor
$d$ foundation penetration depth
$d_{crit}$ peak mobilisation depth in the method of Teh
$d_d$ depth of deviation from a single-layer clay type response (measured from the mudline)
$d_{peak}$ depth of peak position
$d_{punch}$ punch-through depth
$d_{spg}$ height of spigot of spudcan foundation
$d_t$ depth of transition (measured from top of sand)
$E$ clay–sand–clay model parameter
$f_1, f_2$ constant factors in the new conceptual model
$H_c$ height of trapped clay
$H_{ct}$ height of top clay
$H_{eff}$ effective sand height
$H_{fdn}$ height of composite foundation
$H_{plug}$ height of soil plug under foundation
$H_s$ height of sand
$I_D$ sand relative density
$I_R$ relative density index
$K_p$ passive earth pressure coefficient
$m$ Bolton's parameter indicating contribution of dilatancy to sand strength
$N_c$ clay bearing capacity factor
$N_{co}$ bearing capacity factor due to cohesion at the base of a circular foundation
$N_{q,cone}$ bearing capacity factor due to surcharge of a conical foundation
$N_{\gamma,cone}$ bearing capacity factor due to weight of a conical foundation
$p'_o$ mean effective stress
$Q$ total bearing force under a foundation in Teh method
$Q$ natural logarithm of grain crushing strength in kPa
$Q_c$ clay bearing force at the sand–clay interface in the method of Teh
$Q_s$ sand shearing force in the method of Teh
$q_{clay}$ bearing capacity in clay
$q_{clay\text{-}cb}$ bottom clay bearing capacity
$q_{clay\text{-}ct}$ bearing capacity in top clay
$q_d$ bearing pressure at the depth of deviation
$q_{nom}$ nominal bearing pressure
$q_o$ surcharge
$q_{o(s)}$ surcharge on top of sand in clay–sand–clay
$q_{peak}$ peak bearing capacity
$q_{sand}$ sand bearing capacity
$R$ foundation radius
$R, r$ geometric parameters in the method of Teh
$s_u$ undrained shear strength of clay
$s_{ubi}$ bottom sand clay intercept strength in clay–sand–clay
$s_{um}$ undrained clay strength at mudline
$t$ thickness of foundation
$V_f$ volume of foundation
$W$ weight of frustum in Teh method
$W_{SF}$ weight of sand frustum
$z$ vertical coordinate (downward positive)
$\gamma'_{cb}$ bottom clay effective unit weight
$\gamma'_{ct}$ top clay effective unit weight
$\gamma'_s$ sand effective unit weight
$\theta$ skew angle
$\theta_b$ spudcan base angle with horizontal
$\kappa$ strength non-homogeneity or normalised strength gradient
$\mu$ mean value
$\rho_{bt}$ bottom clay undrained shear strength gradient
$\rho_{ct}$ top clay undrained shear strength gradient
$\sigma$ standard deviation
$\sigma'_{hp}$ passive earth pressure
$\sigma'_n$ normal effective stress acting on sides of sand frustum
$\sigma'_z$ effective vertical stress within the sand frustum
$\tau_c$ shear stress at periphery of trapped clay
$\tau_s$ shear stresses in sand
$\phi_{cv}$ constant volume friction angle
$\phi'$ operative friction angle
$\phi^*$ reduced operative friction angle
$\phi_2$ mean of the operative and constant volume friction angle in Teh method
$\psi$ dilation angle
$\psi_t$ geometric parameter representing inclination of slip surface in Teh method

## REFERENCES


Ahmadi, M. M. & Robertson, P. K. (2005). Thin-layer effects on the CPT $q_c$ measurement. *Can. Geotech. J.* **42**, No. 5, 1302–1317.

Baglioni, V. P., Chow, G. S. & Endley, S. N. (1982). Jack-up rig foundation stability in stratified soil profiles. In *Proceedings of offshore technology conference*, Houston, TX, USA, paper OTC 4409, pp. 363–384.

Bolton, M. D. (1986). The strength and dilatancy of sands. *Géotechnique* **36**, No. 1, 65–78, http://dx.doi.org/10.1680/geot.1986.36.1.65.

Dier, A., Carroll, B. & Abolfathi, S. (2004). *Guidelines for jack-up rigs with particular reference to foundation integrity*, Research report 289. Bootle, UK: Health and Safety Executive (HSE).

Drescher, A. & Detournay, E. (1993). Limit load in translational failure mechanisms for associative and non-associative materials. *Géotechnique* **43**, No. 3, 443–456, http://dx.doi.org/10.1680/geot.1993.43.3.443.

Dutt, R. N. & Ingram, W. B. (1984). Jackup rig siting in calcareous soils. *Proceedings of offshore technology conference*, Houston, TX, USA, paper OTC 4840, pp. 541–548.

Hansen, J. B. (1970). *A revised and extended formula for bearing capacity*, Bulletin No. 28. Copenhagen, Denmark: Danish Geotechnical Institute.

Hossain, M. S. (2014). Experimental investigation of spudcan penetration in multi-layer clays with interbedded sand layers. *Géotechnique* **64**, No. 4, 258–276, http://dx.doi.org/10.1680/geot.12.P.194.

Hossain, M. S., Randolph, M. F., Hu, Y. & White, D. J. (2006). Cavity stability and bearing capacity of spudcan foundations on clay. *Proceedings of offshore technology conference*, Houston, TX, USA, paper OTC 17770, pp. 1–18.

Houlsby, G. T. & Martin, C. M. (2003). Undrained bearing capacity factors for conical footings on clay. *Géotechnique* **53**, No. 5, 513–520, http://dx.doi.org/10.1680/geot.2003.53.5.513.

Hu, P., Stanier, S. A., Cassidy, M. J. & Wang, D. (2014a). Predicting peak resistance of spudcan penetrating sand overlying clay. *J. Geotech. Geoenviron. Engng* **140**, No. 2, 04013009.

Hu, P., Wang, D., Cassidy, M. J. & Stanier, S. A. (2014b). Predicting the resistance profile of a spudcan penetrating sand overlying clay. *Can. Geotech. J.* **51**, No. 10, 1151–1164.

Hu, P., Stanier, S. A., Wang, D. & Cassidy, M. J. (2015a). A comparison of full profile prediction methods for a spudcan penetrating sand overlying clay. *Géotechnique Lett.* **5**, No. 3, 131–139.

Hu, P., Stanier, S. A., Wang, D. & Cassidy, M. J. (2015b). Effect of footing shape on penetration in sand overlying clay. *Int. J. Phys. Modelling Geotech.* **16**, No. 3, 119–133.

Hu, P., Wang, D., Stanier, S. A. & Cassidy, M. J. (2015c). Assessing the punch-through hazard of a spudcan on sand overlying clay. *Géotechnique* **65**, No. 11, 883–896, http://dx.doi.org/10.1680/jgeot.14.P.097.

ISO (International Organization for Standardization) (2012). ISO 19905-1: Petroleum and natural gas industries-site specific assessment of mobile offshore units – part 1: jack-ups. Geneva, Switzerland: ISO.

Lee, K. K., Cassidy, M. J. & Randolph, M. F. (2013a). Bearing capacity on sand overlying clay soils: experimental and finite-element investigation of potential punch-through failure. *Géotechnique* **63**, No. 15, 1271–1284, http://dx.doi.org/10.1680/geot.12.P.175.

Lee, K. K., Randolph, M. F. & Cassidy, M. J. (2013b). Bearing capacity on sand overlying clay soils: a simplified conceptual model. *Géotechnique* **63**, No. 15, 1285–1297, http://dx.doi.org/10.1680/geot.12.P.176.

Lunne, T., Robertson, P. K. & Powell, J. M. (1997). *Cone penetration testing in geotechnical practice*. London, UK: Blackie Academic and Professional.

Mandel, J. & Salencon, J. (1969). The bearing capacity of soils on a rock foundation. *Proceedings of the 7th international conference on soil mechanics and foundation engineering*, Mexico City, Mexico, pp. 157–164.

Menzies, D. & Roper, R. (2008). Comparison of jackup rig spudcan penetration methods in clay. *Proceedings of the offshore technology conference*, Houston, TX, USA, paper OTC 19545, pp. 1–22.

Meyerhof, G. G. & Chaplin, T. K. (1953). The compression and bearing capacity of cohesive layers. *Br. J. Appl. Physics* **4**, No. 1, 20–26.

Osborne, J. & Paisley, J. (2002). South east Asia jack-up punch-throughs: the way forward. *Proceedings of the conference on offshore site investigation and geotechnics – sustainability and diversity*, London, UK, pp. 301–306.

Sname (Society of Naval Architects and Marine Engineers) (2008) *Recommended practice for site specific assessment of mobile jack-up units*, 1st edn, T & R Bulletin 5-5A, rev. 3. Alexandria, VA, USA: Society of Naval Architects and Marine Engineers.

Stanier, S. A., Blaber, J., Take, W. A. & White, D. J. (2016). Improved image-based deformation measurement for geotechnical applications. *Can. Geotech. J.* **53**, No. 5, 727–739.

Teh, K. L. (2007). *Punch through of spudcan foundation on sand overlying clay*. PhD thesis, National University of Singapore, Singapore.

Teh, K. L., Cassidy, M. J., Leung, C. F., Chow, Y. K., Randolph, M. F. & Quah, C. K. (2008). Revealing the bearing capacity mechanisms of a penetrating spudcan through sand overlying clay. *Géotechnique* **58**, No. 10, 793–804, http://dx.doi.org/10.1680/geot.2008.58.10.793.

Teh, K. L., Leung, C. F., Chow, Y. K. & Handidjaja, P. (2009). Prediction of punch-through for spudcan penetration in sand overlying clay. *Proceedings of offshore technology conference*, Houston, TX, USA, paper OTC 20060, pp. 1–14.

Teh, K. L., Leung, C. F., Chow, Y. K. & Cassidy, M. J. (2010). Centrifuge model study of spudcan penetration in sand overlying clay. *Géotechnique* **60**, No. 11, 825–842, http://dx.doi.org/10.1680/geot.8.P.077.

Ullah, S. N., Hu, Y., White, D. & Stanier, S. (2014). LDFE study of bottom boundary effect in foundation model tests. *Int. J. Phys. Modelling Geotech.* **14**, No. 3, 80–87.

Ullah, S. N., Stanier, S. A., Hu, Y. & White, D. J. (2017). Foundation punch-through in clay with sand: centrifuge modelling. *Géotechnique* (in press).

Van Den Berg, P., De Borst, R. & Huétink, H. (1996). An eulerian finite element model for penetration in layered soil. *Int. J. Numer. Analyt. Methods Geomechanics* **20**, No. 12, 865–886.

White, D. J., Take, W. A. & Bolton, M. D. (2003). Soil deformation measurement using particle image velocimetry (PIV) and photogrammetry. *Géotechnique* **53**, No. 7, 619–631, http://dx.doi.org/10.1680/geot.2003.53.7.619.